Remote Sensing of Environment 325 (2025) 114773

Contents lists available at ScienceDirect

Remote Sensing of Environment

journal homepage: www.elsevier.com/locate/rse

Use of close-range LiDAR devices and statistical inference approaches in operational stand-level forest inventories

Juan Alberto Molina-Valero [a,b,*], Rorai Pereira Martins-Neto [a], Adela Martínez-Calvo [c], Joel Rodríguez-Ruiz [c], Peter Surový [a], Anika Seppelt [d], César Pérez-Cruzado [c]

[a] Faculty of Forestry and Wood Sciences, Czech University of Life Sciences Prague, Kamýcká 129, 165 00 Prague, Czech Republic
[b] Department of Spatial Sciences, Faculty of Environmental Sciences, Czech University of Life Sciences Prague, Kamýcká 129, 165 00 Prague, Czech Republic
[c] Proyectos y Planificación (PROEPLA), Departamento de Producción Vegetal y Proyectos de Ingeniería, Escuela Politécnica Superior de Ingeniería, Universidade de Santiago de Compostela, Benigno Ledo s/n, Campus Terra, 27002 Lugo, Spain
[d] Faculty of Biology, Albert-Ludwigs-University, Freiburg im Breisgau, Germany

ARTICLE INFO

Edited by Jing M. Chen

Keywords:
Area-based approach
Close-range sensing
Forest management
Forest monitoring
Proximal remote sensing
Statistical sampling

ABSTRACT

Close-range LiDAR devices are considered to have great potential for enhancing forest inventory (FI) estimates. However, this potential is still being explored in the case of ground-based LiDAR devices, especially when the target is focused on relatively large spatial scales, such as stand level. This study explored the performance of close-range LiDAR devices in terms of bias and error, particularly terrestrial laser scanning (TLS) instruments, as measurement tools in stand-level FIs. The main premise of the research is that close-range LiDAR devices provide auxiliary information that can be used to accurately and precisely predict the dependent variable of the target population, thereby reducing errors. To this end, this study compared the performance of different statistical inference approaches that can be implemented with these technologies, such as the simple expansion estimator (EXP), two-stage model-assisted regression (REG), conventional model-based (CMB) and three-phase hierarchical model-based (3pHMB) approaches. These approaches were used to compare the following types of data: field measurements and TLS single-scan data (EXP, REG); field measurements and unmanned aerial vehicles (UAV)-LiDAR data (CMB); and field measurements, TLS single-scan data and UAV-LiDAR data (3pHMB). The case study was carried out in a 16 ha experimental plot dominated by *Pinus radiata* and *Pinus pinaster* in northwest Spain, focusing on stand volume (V, $m^3\ ha^{-1}$) estimates. The findings showed that the use of close-range remote sensing devices as a source of auxiliary data provided lower error in V estimates than the EXP approach using a single data source. The findings also suggest that close-range LiDAR devices can potentially be used as FI instruments. Therefore, the transfer of these sampling techniques may play an important role in operationalizing the use of close-range LiDAR devices in FIs.

1. Introduction

Forest inventories (FIs) have improved since they were first introduced, owing to the continuous emergence of new technologies, especially in the last few decades since the advent of remote sensing (Fassnacht et al., 2023; White et al., 2016). While conventional FIs are costly and time-consuming, the use of remote sensing can increase both the spatial scale and frequency of estimates without a proportional increase in the associated costs (Coops et al., 2023; Kangas et al., 2018). In this technological context, light detection and ranging (LiDAR) systems provide three-dimensional point clouds, which are suitable for estimating tree attributes and are very useful for many forestry applications (Dubayah and Drake, 2000). Indeed, the operational feasibility of LiDAR for estimating essential FI variables at stand level, including timber volume (V, $m^3\ ha^{-1}$), with airborne laser scanning (ALS) and unmanned aerial vehicle (UAV)-LiDAR devices has been demonstrated (Puliti et al., 2015; White et al., 2016; Wulder et al., 2012). Among close-range LiDAR devices, ground-based instruments such as terrestrial and mobile laser

This article is part of a Special issue entitled: 'CRS-Forests' published in Remote Sensing of Environment.

* Corresponding author.
E-mail addresses: molina_valero@fld.czu.cz (J.A. Molina-Valero), pereira_martins_neto@fld.czu.cz (R.P. Martins-Neto), adela.martinez.calvo@usc.es (A. Martínez-Calvo), joel.ruiz@usc.es (J. Rodríguez-Ruiz), surovy@fld.czu.cz (P. Surový), cesar.cruzado@usc.es (C. Pérez-Cruzado).

https://doi.org/10.1016/j.rse.2025.114773
Received 18 April 2024; Received in revised form 12 March 2025; Accepted 19 April 2025
Available online 30 April 2025

scanning (TLS and MLS, respectively) instruments provide high-resolution point cloud data that show great potential for enhancing FIs (Dassot et al., 2011; Fassnacht et al., 2023; White et al., 2016) and forest ecology research (Calders et al., 2020). One of the main advantages of using TLS or MLS data is that they provide better observations of near-ground vegetation than airborne systems (Lovell et al., 2003), which may be an advantage for estimating *V* as one of the variables most frequently predicted in FIs, especially when predicted from LiDAR data (Coops et al., 2021). These types of data also have several key advantages over traditional field data, such as non-invasive measurements and automatically-acquired data (Krok et al., 2020). However, TLS and MLS devices have not yet been adopted in FIs for several reasons: (1) the difficulty in automating data processing to obtain reliable predictors and estimates of important forest variables; (2) high acquisition costs; (3) limited software; (4) lack of trained personnel (Liang et al., 2016); and (5) possible bias in tree-level estimates (Abegg et al., 2023). Many researchers agree that affordability is the main key challenge to overcome, emphasizing that automation of point cloud processing with affordable and easy-to-use software capable of extracting information related to important forest attributes is essential (Dassot et al., 2011; Liang et al., 2016, 2018; Newnham et al., 2015; White et al., 2016).

While ground-based technologies can provide accurate estimates, e.g. of tree diameters, close to what is required in practical applications, this is conditioned by factors such as occlusions, tree size and the structural complexity of the forest (Liang et al., 2018). For instance, volume estimates for small trees have been found to be highly biased (Abegg et al., 2023), as have volume estimates in structurally complex near-natural mixed forests (Vatandaşlar et al., 2023). Despite these limitations, such technologies also enhance conventional data collection by enabling measurement of variables that are more challenging to assess (Calders et al., 2020), which is probably why they have been classified as important tools at tree level (Srinivasan et al., 2015), plot level (Newnham et al., 2015) and for characterization of small stands (Trochta et al., 2017). Nevertheless, there are fewer examples of their role in FIs beyond replacing conventional measurement plots (Kuželka et al., 2022). Their potential as sampling tools has scarcely been explored in statistical sampling other than in design-based, single-phase sampling approaches. In addition to the technical capacities, ground-based LiDAR devices have features that are well suited to operational FIs and monitoring programs, including the following: (1) objectivity of measurement and therefore better quality control (e.g. applicable in audits); and (2) the possibility of recording long-term time series, which become more valuable over time, as retrospective analysis of the data will provide additional attributes through algorithm improvements (Fassnacht et al., 2023). However, the potential of ground-based LiDAR devices as measurement instruments to enhance operational FIs at stand level (e.g. for management purposes) or larger scales has scarcely been explored. The few examples of such studies include the use ground-based LiDAR technology to replace field measurements in combination with other remote sensing techniques (Persson et al., 2022), the use of ground-based LiDAR estimates through distance sampling approaches with TLS single-scans (Astrup et al., 2014; Ducey and Astrup, 2013); Kriging predictions from MLS (i.e. model-based inference) corrected for undetected trees based on distance sampling theory (Saarela et al., 2017) and the construction of allometric models to upscale volume predictions from TLS to ALS (Luck et al., 2023). Most challenges in management-level FIs are currently related to how to further optimize existing workflows by integrating ground-based laser scanning approaches (Fassnacht et al., 2023). Nevertheless, for scales such as management-level FIs and National Forest Inventories (NFIs), the use of these devices as sources of auxiliary information in combination with sample field data (or similar) may have pragmatic, operational applications.

Some of the above technical operational requirements have been successfully covered by different area-based approaches (ABAs) such as model-based inference techniques. In these methods, full coverage of remotely sensed auxiliary information is used to fit predictive models with field data samples obtained without any assumptions about the sampling design (Gregoire, 1998; McRoberts, 2006), or with partial coverage of auxiliary information data collected as a probability sample in the case of hybrid inference (Corona et al., 2014). This approach has been used to estimate, for example, the proportion of forest area from Landsat imagery (McRoberts, 2006, 2010) or common variables in FIs including ALS data (Guerra-Hernández et al., 2022); in both cases full coverage of auxiliary information data is used. The model-based inference approach has also been used to estimate above-ground biomass (*AGB*) by using ALS strips as partial coverage of auxiliary information (Andersen et al., 2011), among many other variables. Other examples of the approach include model-assisted inference techniques, which are based on the use of remotely sensed auxiliary information data in combination with probabilistic sampling of field data (Särndal et al., 1992). In this case, there are also examples of (1) studies using full coverage of auxiliary information data, e.g. provided by ALS data for estimating *V* (Strunk et al., 2012); and (2) studies using partial coverage of auxiliary information data, e.g. by ALS strip sampling, which are successfully used to estimate *AGB* (Gregoire et al., 2011; Næsset et al., 2013). Finally, a hierarchical inference approach in which estimates are calculated from multiple sources of information has also recently been proposed (Massey et al., 2014; Saarela et al., 2023). These various sources of auxiliary information data can be directly applied if they are based on probability samples, by following the established theory for model-assisted approaches (Särndal et al., 1992), e.g. for estimating growing stock volume (Saarela et al., 2015a). Furthermore, Saarela et al. (2016) developed a hierarchical model-based inference estimation framework in which the main advantage is that estimators do not require probability samples for the auxiliary information data sources used. An example of the latter type of study, which combines the use of UAV with LiDAR technology and Sentinel-2 imagery as auxiliary information data, together with field (plot) data, to estimate *V*, is reported by Puliti et al. (2018). Nevertheless, to the best of our knowledge, case studies using ground-based LiDAR as sources of auxiliary information data are non-existent.

The main objectives of the study were as follows: (1) to analyze the usefulness of various of close-range LiDAR devices in FIs at stand level; (2) to compare different estimators and modes of inference such as simple expansion estimator (EXP), two-stage model-assisted regression (REG), conventional model-based (CMB) and three-phase hierarchical model-based (3pHMB) approaches; and (3) to assess the performance of the different inference approaches, simulating different sampling designs and intensities. For these purposes, the following information sources were compared: (1) field measurements and TLS single-scans for EXP inference, (2) field measurements and TLS single-scans for REG inference, (3) field measurements and UAV-LiDAR coverage for CMB inference, and (4) all data sources for 3pHMB inference. The study was conducted by adopting the EXP approach with field measurements as the baseline and using Monte Carlo simulations to estimate the uncertainty of estimates. The work focused on estimating *V* to assess all of the established objectives.

2. Material

2.1. Study area

The study area comprises a communal woodland located in northwest Spain (Galicia). The woodland mainly consists of radiata pine (*Pinus radiata* D. Don) and maritime pine (*Pinus pinaster* ssp. *atlantica* H. de Vill), which reach densities of 63 % and 19 % respectively, with other species (*Quercus robur* L., *Quercus pyrenaica* Willd., *Castanea sativa* Mill. and *Betula* spp.) accounting for the remaining 18 %. The study site covers an area of 16 ha (400 × 400 m) and harbours several stands representing different stages of development due to the silvicultural rotation forest management scheme implemented. The study area was

tessellated into 400 square grid cells of size of 20 × 20 m. As in most studies using these sampling techniques, the plot design consisted of N_U = 400 circular plots of 10 m radius (314.16 m^2) inscribed in each cell. Therefore, the N_U plots constituted the study target population U. All cells were sampled by conventional field-based measurement, TLS single-scans and a wall-to-wall UAV-LiDAR flight (Fig. 1).

2.2. Field data

A stand census, which consisted of geolocating and measuring all trees taller than 1.3 m, was conducted in 2021. The topographical bases from which tree positions were surveyed, were collected using a GPS (Trimble R2) with sub-centimetre precision. From these, tree positions were surveyed with a laser technology device (TruPulse 360°R) using azimuths and horizontal distances with a precision of 0.1° and 0.1 m, respectively. The diameter at breast height (*dbh*, cm, diameter at 1.3 m above ground level) of each tree was measured (to the nearest 0.1 cm) with calipers and reported as the average of two measurements in perpendicular directions. The total tree height (h, m) was measured to the nearest 0.1 m with a digital hypsometer (Vertex IV, Haglöf Sweden). The stem volume of the trees was estimated using local species-specific tree allometric models with *dbh* and h as predictive variables (Diéguez-Aranda et al., 2009). The stand-level stem volume (V, m^3 ha^{-1}) was then estimated by aggregating the volumes of individual trees and expanded to area units (ha), which enabled us to determine the true value of the population mean parameter considered in this study (μ = 254.42 m^3 ha^{-1}). This reference value was obtained from the 400 circular plots of 10 m radius (N_U) inscribed in each of the grid cells (simulated on the basis of field data) to be used as sampling units. Therefore, 400 predicted values of V at plot level were obtained, providing an overall insight into the population of interest, which consisted of 5,012 trees. The values of the main stand-level (or dasometric) variables are shown in Table 1.

2.3. Remotely sensed data

2.3.1. TLS

The sampling design consisted of a 20 × 20 m systematic regular grid (400 sampling points) in which single scans were conducted (Fig. 1). A terrestrial laser scanner (TLS) *FARO Laser Scanner Focus3D X 130* device was used to scan the 400 plots from the sampling points allocated, covering the full horizontal (0–360°) and vertical (−60–90°) ranges with a resolution of 7.67 mm at 10 m in both horizontal and vertical angular apertures. TLS single-scans were then systematically processed with the

Table 1
Mean and standard deviation (in parentheses) for stand-level variables.

Species	N (trees ha^{-1})	G (m^2 ha^{-1})	V (m^3 ha^{-1})	$\overline{d}$ (cm)	$\overline{h}$ (m)
P. radiata	253 (144)	19.7 (12.3)	212 (156)	31.1 (9.6)	22.6 (6.4)
P. pinaster	74 (86)	4.7 (6.1)	35 (48)	27.3 (8.2)	15.9 (5.0)
Other species	73 (240)	1.1 (3.4)	7 (25)	12.5 (5.8)	10.4 (4.0)
Total	400 **(247)**	**25.6 (11.8)**	**254 (150)**	**28.1 (8.6)**	**20.1 (6.1)**

All values were estimated from the 400 (N_U) circular plots of 10 m radius inscribed in each squared grid cells of 20 m side, thus sampling the whole population. N, number of trees per hectare (trees ha^{-1}); G, stand basal area (m^2 ha^{-1}); V, stem volume (m^3 ha^{-1}); $\overline{d}$, mean diameter (cm); and $\overline{h}$, mean height (m). The values of N and V have been rounded to unity.

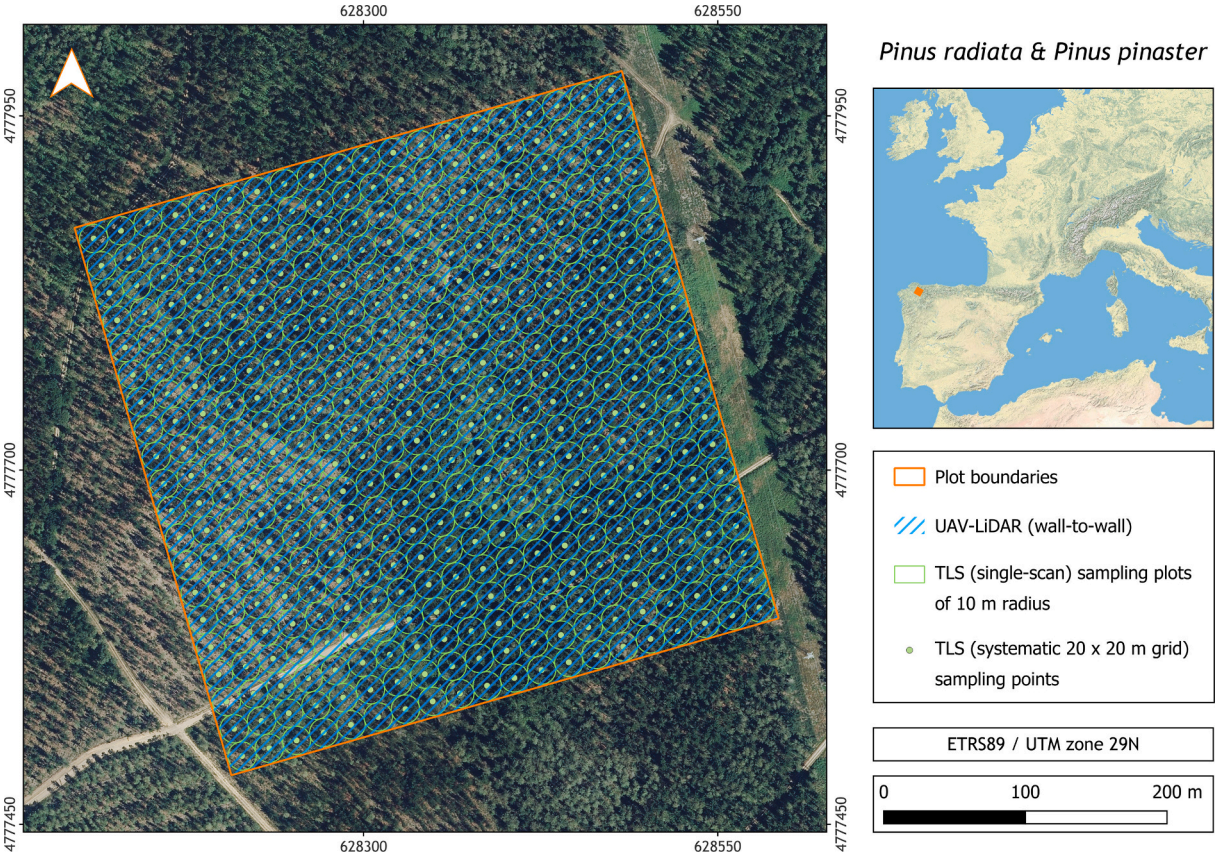

Fig. 1. Overview of the study area, wall-to-wall UAV-LiDAR flight and sampling design adopted for TLS single-scans with 10 m radius plots established at the centres of 20 × 20 m cells. The field data were obtained by census of the whole stand.

FORTLS package (Molina-Valero et al., 2022) in the free software environment R (R Core Team, 2023), considering circular fixed area plots of radius 10 m. In the processing, ground points were classified using the Cloth Simulation Filter (CSF) algorithm (Zhang et al., 2016), and a digital terrain model (DTM) was generated by spatial interpolation with a k-nearest neighbor approach using inverse distance weighting at a resolution of 0.2 m. The DTM was then used to normalize the point clouds by adjusting point elevations relative to the ground level. These processes are included by default in the *FORTLS* package. The processing yielded stand-level variable estimates (e.g. for stand volume, Table A.1) and also metrics such as height percentiles (m) derived from the z coordinates of the point clouds (Table A.2). Hereinafter, these variables and metrics are referred to as TLS auxiliary data when used as auxiliary information for fitting the models required for REG and 3pHMB approaches. Accordingly, the proposed sampling design allowed us to generate wall-to-wall TLS single-scan data, thus producing TLS auxiliary data for the N_U plots of the target population U. In the case of the EXP approach with TLS data, both direct V estimates (V.tls, Table A.1) and corrected estimates based on occlusion effects (V.sh, V.hn, V.hn.cov, V.hr and V.hr.cov, Table A.1) were used to estimate the mean population μ. The latter approaches are based on distance sampling methods (V.hn, V.hn.cov, V.hr and V.hr.cov, Buckland et al., 2001) and correction of the shadowing effect (V.sh, Seidel and Ammer, 2014).

Distance sampling methods were implemented through the point transects method, which uses detection functions $g(r,\theta)$ with the explanatory variable r (distance from sampling point) and parameter θ to describe how the probability of tree detection decreases as distance increases. Both half-normal and hazard-rate functions were used as these have been successfully used to estimate V from TLS data (Astrup et al., 2014). Once the parameters of detection functions are estimated, the probability of tree detection in the sample area (P_i) is estimated as follows:

$$\widehat{P}_i = \frac{2}{R^2}\int_0^R rg(r,\widehat{\theta})dr \tag{1}$$

where R is the plot radius. Therefore, $\widehat{P}_i$ is the estimated unconditional probability of detecting a tree within the circular plot, and can be used to increase the expansion factor in the estimation of stand-level variables as follows:

$$\widehat{V}_{corrected,i} = \widehat{V}_i \bullet \frac{1}{\widehat{P}_i} \tag{2}$$

where $\widehat{V}_i$ is the volume estimated for each detected tree i in units of volume per unit area (e.g. $m^3\ ha^{-1}$), and $\widehat{V}_{corrected,i}$ is the corrected volume estimate after applying the previously outlined approach. On the other hand, the shadowing effect caused by occlusions was corrected in order to eliminate the unsampled shaded area (A_{sh}) related to the total plot area, as follows:

$$A_{sh} = \sum_i \left[\frac{(\pi R^2) - (\pi {r_{tree,i}}^2)}{360^\circ} \bullet tan^{-1}\left(\frac{dbh_i}{r_{tree,i}}\right) - \frac{\pi\left(dbh_i/2\right)^2}{2} \right]_i \tag{3}$$

where R is the radius of the plot, $r_{tree,i}$ is the distance between the TLS instrument and the tree centre for each detected tree i, and dbh_i is the dbh value; both $r_{tree,i}$ and dbh_i are expressed in the same units as R. A_{sh} can be deducted from the total plot area, thus generating a more realistic sampling area, to increase the expansion factor in the estimation of stand-level variables as follows:

$$\widehat{V}_{corrected} = \widehat{V} \bullet \left(1 + \frac{A_{sh}}{\pi R^2}\right) \tag{4}$$

where $\widehat{V}$ is the estimation of volume per unit area, and $\widehat{V}_{corrected}$ is the corrected volume estimate after correcting for the shadowing effect.

2.3.2. UAV-LiDAR

Wall-to-wall UAV-LiDAR data were captured in May 2021 with a Phoenix Aerial Scout-16 system, which combines the LiDAR Velodyne VLP-16 puck sensor with a Dual-Antenna moving baseline RTK. The lightweight system (1.85 kg) was mounted aboard a DJI S900 UAV hexacopter (Phoenix LiDAR Systems, 2020). The flight height was 70 m and the dual-return mode was selected, so that for each pulse emitted, up to two returns (first and last) were recorded. The resulting 3D point cloud has an average density of 577 points m^{-2}.

The aerial point cloud was used to calculate LiDAR metrics for the N_U plots of the target population U. In this step, the *lidR* (Roussel and Auty, 2023; Roussel et al., 2020) and *lidRmetrics* (Tompalski and Goodbody, 2021) packages in the R environment were used. First, the outliers from the point cloud were removed using the Statistical Outlier Removal (SOR) algorithm. Subsequently, the point cloud was classified into ground and non-ground points (i.e. vegetation) using the Progressive Morphological Filter (PMF) algorithm (Zhang et al., 2003). Since the study area does not present significant complexity for either outlier removal or point classification, the default values from the *lidR* package were used. The ground points were rasterized using the triangular irregular network to generate the DTM with a ground sample distance of 0.25 cm. The DTM was subtracted from the vegetation points thus normalizing the height of the point cloud. The LiDAR metrics were then calculated from the normalized point cloud at plot level using a vector file containing 400 plots (N_U) with a radius of 10 m and the centres coinciding with field-based and TLS single-scan plot centres. The set of LiDAR metrics calculated per plot is shown in Table A.3.

3. Methods

3.1. Statistical inference approaches

Different assumptions were applied in the four inferential methods used in this study: simple expansion estimator (EXP); two-stage model-assisted regression (REG); conventional model-based (CMB); and three-phase hierarchical model-based (3pHMB). On one hand, both EXP and REG, which are design-based inference approaches, require fulfillment of the following three assumptions: "(1) population units are sampled using a probability-based randomization scheme; (2) the probability of selection for each population unit into the sample is positive and known; and (3) the observation of the response variable for each population unit is a constant" (McRoberts et al., 2014). On the other hand, the following three assumptions must be fulfilled for CMB and 3pHMB, which are model-based inference approaches: (1) observation of the variable of interest for a population unit is a random variable whose values are considered a realization from an underlying distribution (i.e. not a constant); (2) the basis for the inference is the model of the relationship between the response variable and the explanatory variables, not the probabilistic nature of the sample; and (3) randomization enters through the random realizations from the distribution for populations units, rather than the random selection of the population units to be included in the sample. One important consequence of these assumptions is that probability samples may be used with the latter two of the above-mentioned inference approaches although they are not required, making them compatible with the first two (McRoberts et al., 2014). Although estimators based on the previous approaches were used in this study to estimate the population mean parameter μ of interest, Monte Carlo simulations were computed to estimate uncertainty measures in all cases, instead of considering the most usual estimators based on analytical expressions.

The whole study area was measured (i.e. censused) to produce field data and scanned by remote sensing, thus enabling simulation of

different intensities and sampling designs, which can be classified according to the number of sources of information used, as follows: (1) one source formed by either field data or TLS data; (2) two sets of sources, i.e. TLS and field data, and wall-to-wall UAV-LiDAR and field data; and (3) three sources represented by wall-to-wall UAV-LiDAR, TLS and field data (Fig. 2).

Simple random sampling (SRS) without replacement was used as one of the selection methods in all inference approaches. However, for those approaches using auxiliary remotely sensed data (TLS and UAV-LiDAR), the local pivotal method (LPM) was also used to select balanced samples based on auxiliary variables (Deville and Tillé, 1998; Grafström et al., 2012). This method generates representative samples of the auxiliary variable space, which provides samples spread over the correlated response variable (i.e. representative samples) (Tillé and Wilhelm, 2017). One of the advantages of the LPM is that the samples generated are probabilistic, with either equal (the case of this work) or unequal inclusion probabilities (Grafström et al., 2014), thus fulfilling the design-based sampling assumptions. However, equal inclusion probabilities in the selection of population units guarantee well spread and representative samples, as opposed to unequal inclusion probabilities, which may be well spread but not representative (Grafström and Schelin, 2014). For this study, V.tls (Table A.1) and zq_{95} (Table A.3) were used as auxiliary variables for LPM sampling based on TLS and UAV-LiDAR data, respectively, because they were closely correlated with *V*.

3.1.1. Simple expansion estimator (EXP)

EXP is a statistical technique based on SRS, in which the selected samples are used to estimate the population parameters (Cochran, 1977; Särndal et al., 1992). Samples (*S*) were randomly selected using SRS, without replacement from grid cells, with the observational design being a circular plot of 10 m radius. For every plot, *V* was estimated at plot-level by aggregating the volume of individual trees within the plot and expanding the resulting value to area units (ha). Estimates of *V* based on both field data and TLS single-scan data were considered. As previously explained, *V* estimates were obtained in the former case by means of allometric models, and in the latter case by processing the scanning data with the R package *FORTLS* to compute direct (V.tls) and corrected estimates (V.sh, V.hn, V.hn.cov, V.hr and V.hr.cov, see Table A.1) of *V*. In EXP inference, the population mean parameter (μ) for the variable of interest is estimated using the unbiased estimator arithmetic mean $\widehat{\mu}_{EXP}$ (Eq. (5)) as follows:

$$\widehat{\mu}_{EXP} = \frac{1}{n}\sum_{i \in S} y_i \tag{5}$$

where i represents the n observations in sample S, and y_i is the observation (*V* estimate based on field data or TLS data, in this study) for the *ith* population unit in the sample.

3.1.2. Two-stage model-assisted regression (REG)

In two-stage sampling designs, the population is tessellated into first-stage population units which, in turn, are tessellated into second-stage population units (McRoberts et al., 2024). Samples are then drawn at both stages by random sampling. The REG estimator uses models based on auxiliary data to enhance inference but rely on probability samples for validity (McRoberts et al., 2014). In this study, REG was applied in those cases in which the auxiliary data were generated by single-scan TLS, and the conventional field data supported the forest attribute *V*. In the case applied here, a relationship between the response variable y and a vector $\boldsymbol{x}$ of explanatory variables (field-based *V* estimates and TLS auxiliary data, respectively, in this work) was modelled as follows:

$$y_i = f(\boldsymbol{x}_i;\boldsymbol{\beta}) + \varepsilon_i \tag{6}$$

where $f(\boldsymbol{x}_i;\boldsymbol{\beta})$ expresses the mathematical relationship between the explanatory variables and the model parameters; $\boldsymbol{\beta}$ is a vector of the p model parameters to be estimated; and ε_i is a random residual assumed to be distributed as $\varepsilon_i \sim N(0, \sigma_i^2)$. It should be noted that $f(\boldsymbol{x};\boldsymbol{\beta})$ can be formulated by means of a linear or nonlinear models (Firth and Bennett, 1998).

Cases were evaluated in which coverage of the auxiliary data was partial relative to the total population, following "Case C" in Särndal et al. (1992, p. 323). This consisted of taking a first-stage sample from N_U with auxiliary information (S_1) of a relatively large size n_1 implemented using SRS without replacement. A second-stage sample (S_2) of size n_2 ($n_2 < n_1$) consisting of a subsample of S_1 was then obtained by means of an arbitrary probability sampling design. Sample S_2, with pairwise data corresponding to response and explanatory variables (field-based *V* estimates and TLS auxiliary data) was used to fit the model relationship (Eq. (6)). In this case, and under SRS assumptions, the regression estimator for the population mean μ (Eq. (7)) was

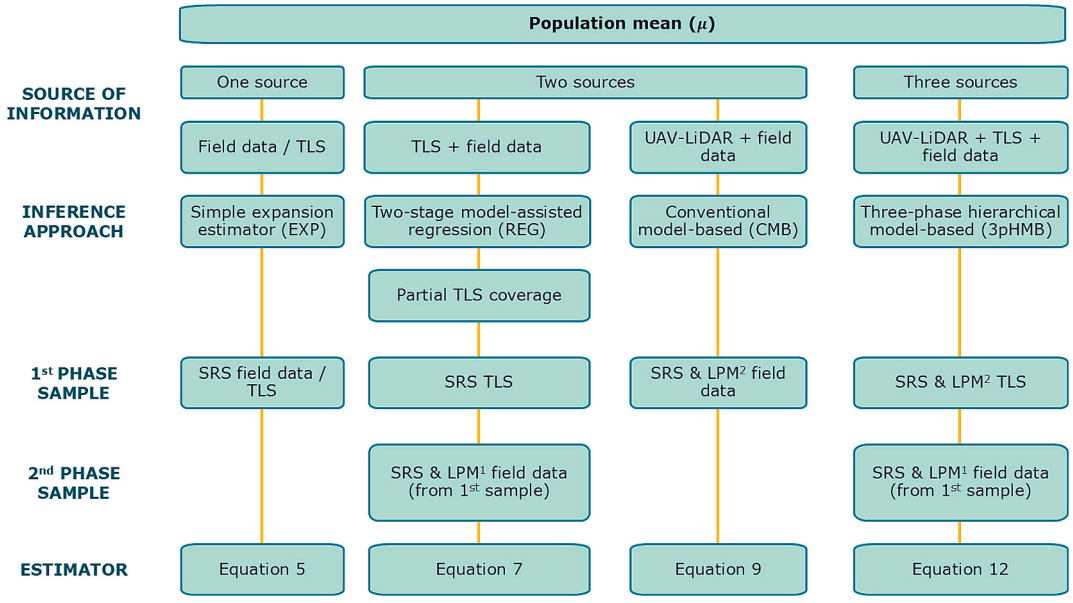

Fig. 2. Inference approaches and sampling designs used in the study, organized according to the source of information and inference approach used. [1]LPM sampling based on TLS sample auxiliary variable space (V.tls, Table A.1). [2]LPM sampling based on UAV-LiDAR auxiliary variable space (zq_{95}, Table A.3).

obtained from McRoberts et al. (2024), who derived the Särndal estimators (Särndal et al., 1992, p. 323) using the more familiar Cochran-like notation, as follows:

$$\widehat{\mu}_{reg} = \frac{1}{n_1}\sum_{i\in S_1}\widehat{y}_i + \frac{1}{n_2}\sum_{i\in S_2}(y_i - \widehat{y}_i) \quad (7)$$

where $\widehat{y}_i$ is the forest attribute V predicted according to the regression model (Eq. (6)). This estimator is approximately design-unbiased, irrespective of the model choice when n_2 is not too small (Särndal et al., 1992).

In order to select S_2, two different probabilistic criteria were considered: SRS without replacement and the LPM described in Grafström et al. (2012) using TLS auxiliary information to select balanced samples. For the latter, the stand volume estimated using the R package *FORTLS* (V.tls, see Table A.1) was used as auxiliary information for selecting S_2 in the R package *BalancedSampling* (Grafström et al., 2022). As already mentioned, this variable was considered because of its high correlation with V, as this approach benefits from the correlation between the variable of interest and the auxiliary information (Fig. A.1). Both sampling procedures (SRS and LPM) were explored in this study to assess possible differences in estimates and the associated errors.

3.1.3. Conventional model-based (CMB)

One of the main advantages of the model-based approach is that probability sampling is not necessary, as it is based on the concept of a superpopulation model, in which any finite population of interest is seen as a sample drawn from a larger universe defined by the superpopulation model (Cassel et al., 1977). There is therefore a relationship between the mean of the distribution from which observations for population units are generated (μ_i) and the vector $\boldsymbol{x}$ of explanatory variables (formed by UAV-LiDAR auxiliary data in this case), which can be expressed as follows:

$$\mu_i = f(\boldsymbol{x}_i;\boldsymbol{\beta}) + \varepsilon_i \quad (8)$$

where $f(\boldsymbol{x}_i;\boldsymbol{\beta})$ expresses the mathematical relationship between the explanatory variables and the model parameters; $\boldsymbol{\beta}$ is a vector of the p model parameters to be estimated; and ε_i is unexplained residual uncertainty assumed to be distributed with zero mean. Following the established theory (Matérn, 1960; McRoberts, 2006) and the most recent notation (Saarela et al., 2018), the CMB estimator of the population mean μ (Eq. (9)) is defined as follows:

$$\widehat{\mu}_{CMB} = \frac{1}{N_U}\sum_{i\in U}\widehat{\mu}_i \quad (9)$$

where $\widehat{\mu}_i = f(\boldsymbol{x}_i;\widehat{\boldsymbol{\beta}})$ is the model prediction for population parameter of interest, and where $\widehat{\boldsymbol{\beta}}$ is the vector containing the model parameter estimates. The principles of CMB inference were used to estimate the population mean in the target fixed population of this study and obtain associated uncertainty measures through Monte Carlo procedure described below. Hence, the results obtained were labelled as CMB although the approach in this manuscript differs from the usual one in model-based contexts. Specifically, as in previous cases with auxiliary information, both SRS without replacement and LPM were used to select a sample S of size n (field-based V estimates and UAV-LiDAR auxiliary data, in this case) to fit the model in Eq. (8). For LPM sampling, UAV-LiDAR auxiliary data were also used to select spatially balanced field samples in the auxiliary variables space, and the 95th percentile of z coordinates of point clouds (zq_{95}, see Table A.3) was used as auxiliary information. This variable is considered because it is closely correlated with V (Fig. A.1), as this approach benefits from the correlation between the variable of interest and the auxiliary data.

3.1.4. Three-phase hierarchical model-based (3pHMB) approach

This approach shares the same assumptions as the CMB approach, but several sources of auxiliary information are used for inference instead of only one (Saarela et al., 2016, 2023). The first-phase source of information corresponded to UAV-LiDAR data, which were available for all population elements (N_U). The second-phase source of information corresponded to a first-phase sample of n_1 grid cells measured by TLS single-scans, denoted as S_1. Thus, each grid cell in S_1 had two sets of auxiliary data available, UAV-LiDAR data and TLS data. The third-phase source of information was a subsample of n_2 grid cells selected from S_1 and measured by conventional field data, denoted S_2. Hence, for each element in S_2, UAV-LiDAR data, TLS data and V estimates were available. As in previous cases with auxiliary information, both SRS without replacement and LPM were implemented to select samples S_1 and S_2 in a hierarchical manner, always using the larger sample as an auxiliary information source for selecting balanced samples in the case of the LPM approach. The auxiliary variables used were the same as in the previous cases, with zq_{95} for S_1 and V.tls for S_2. According to sub-case C.2 presented in Saarela et al. (2016) and developed more rigorously in Saarela et al. (2023), two models were considered, as follows. The first model corresponds to the relationship between the mean of population units (μ_i) and the vector $\boldsymbol{x}$ of explanatory variables derived from the second-phase source of information, that can be expressed as follows:

$$\mu_i = f_x(\boldsymbol{x}_i;\boldsymbol{\beta}_{\boldsymbol{x}}) + \varepsilon_{\boldsymbol{x},i} \quad (10)$$

where $f_x(\boldsymbol{x}_i;\boldsymbol{\beta}_{\boldsymbol{x}})$ links the explanatory variables and the p_X model parameters contained in the vector $\boldsymbol{\beta}_{\boldsymbol{x}}$; and $\varepsilon_{\boldsymbol{x},i}$ is a random deviation with mean equals to zero. The model in Eq. (10) is fitted with S_2, by using TLS auxiliary data as explanatory variables and V estimated with field-based data as the response variable. This model is used to predict population mean for all elements in S_1 as $\widehat{\mu}_{x,i} = f_X(\boldsymbol{x}_i;\widehat{\boldsymbol{\beta}}_{\boldsymbol{x}})$, being $\widehat{\boldsymbol{\beta}}_{\boldsymbol{x}}$ the model parameter estimates. On the other hand, a second model expressing the relationship between $f_x(\boldsymbol{x}_i;\boldsymbol{\beta}_{\boldsymbol{x}})$ and the vector $\boldsymbol{z}$ of explanatory variables related to the first source of information is expressed as follows:

$$f_x(\boldsymbol{x}_i;\boldsymbol{\beta}_{\boldsymbol{x}}) = f_{\boldsymbol{z}}(\boldsymbol{z}_i;\boldsymbol{\beta}_{\boldsymbol{z}}) + \varepsilon_{\boldsymbol{z},i} \quad (11)$$

where, again, $f_{\boldsymbol{z}}(\boldsymbol{z}_i;\boldsymbol{\beta}_{\boldsymbol{z}})$ represents the link between $\boldsymbol{z}$ and the p_z elements of the model parameter vector ($\boldsymbol{\beta}_{\boldsymbol{z}}$); and $\varepsilon_{\boldsymbol{z},i}$ is a zero-mean random deviation. This second model (Eq. (11)) is fitted using the model predictions $\widehat{\mu}_{\boldsymbol{x},i}$ for all $i \in S_1$ as the response variables and UAV-LiDAR data for S_1 as explanatory variables. The fitted model was then applied to predict all population elements to obtain the 3pHMB estimator of the population mean μ (Eq. (12)), as follows:

$$\widehat{\mu}_{3pHMB} = \frac{1}{N_U}\sum_{i\in U}\widehat{\mu}_{\boldsymbol{z},i} \quad (12)$$

where $\widehat{\mu}_{\boldsymbol{z},i} = f_{\boldsymbol{z}}(\boldsymbol{z}_i;\widehat{\boldsymbol{\beta}}_{\boldsymbol{Z}})$ is the model prediction for each population unit based on the model parameter estimates $\widehat{\boldsymbol{\beta}}_{\boldsymbol{Z}}$. As commented in the case of CMB, 3pHMB notation was maintained in the results derived from this approach, even though Monte Carlo simulations were used to obtain uncertainty measures.

3.2. Model fitting

As the objective was not to obtain superpopulation models, but to simulate realistic cases of operational FIs at stand level, we decided to fit the models in each sample selection simulation under the assumption that the hypothetical forester has no prior knowledge of the stand. In particular, linear regression models that were as simple as possible (Eq. (13)) were fitted, also in order to easily automate all the simulations, including up to 3 explanatory variables in more complex cases:

$$y_i = \beta_0 + \beta_1 x_{1_i} + \ldots + \beta_{p-1} x_{p-1_i} + \varepsilon_i \quad (13)$$

where y is the response variable and $x_1, \ldots, x_{p-1}$ are the explanatory variables (field-based or model-based V estimates as response variable,

and TLS or UAV-LiDAR auxiliary data as explanatory variables, depending on the inference approach or inventory phase); $\beta_0, \ldots, \beta_{p-1}$ are the parameters to be estimated; and $\boldsymbol{\varepsilon}$ is the model residuals vector. To accommodate heteroskedasticity and following previous studies, such as that conducted by Breidenbach et al. (2016), weighted models were fitted, where each observation in the regression model was weighted by the inverse of the explanatory variables, as the residual variances were proportional to these.

The process for selecting variables consisted of the following steps: (1) preselection of those variables most closely correlated with the response variable (with a Pearson correlation coefficient (ρ) higher than 0.5), i.e. the explanatory variables most likely to explain the response variable; (2) implementing a hierarchical cluster analysis method, complete-linkage clustering, to find 5 clusters of variables and then selecting those variables with highest ρ with the response variable from each group, to avoid autocorrelation among explanatory variables; and (3) based on previous selection of variables, an exhaustive search for the best subsets of the explanatory variables for predicting the response variable in linear regression was performed, using an efficient branch-and-bound algorithm implemented in the function *leaps* from the homonymous R package (Lumley, 2020).

3.3. Analyses

Since there was access to the entire population units (N_U) for all sources of data, we decided to use Monte Carlo sampling simulation to assess bias ($\widehat{Bias}(\hat{\mu})$) and standard error ($\hat{se}_{\hat{\mu}}$). Another reason we decided to use Monte Carlo simulation was because with 3pHMB inference, there is still no analytical expression of variance that includes autocorrelation issues (Saarela et al., 2023). For this purpose, the first step was to randomly resample the original data without replacement. Depending on the inference approach used, the following patterns can be distinguished: (1) for EXP and CMB inference approaches, this process was conducted for different field sample sizes ($n = 10, 11, \ldots, 50$); (2) for the REG approach, three sampling intensities for S_1 ($100 \bullet n_1/N_U$) in partial auxiliary data coverage were considered (75 %, 50 % and 25 %; corresponding to $n_1 = 300, 200, 100$, respectively), as well as a progressive increase for the second-stage sample S_2 in the partial coverage from $n_2 = 10$ to $n_2 = 50$ ($n_2 = 10, 11, \ldots, 50$); (3) for the 3pHMB approach, three sample sizes of S_1 were considered ($n_1 = 300, 200, 100$), which correspond to sampling intensities ($100 \bullet n_1/N_U$) of 75 %, 50 % and 25 %, respectively; as well as a progressive increase in the S_2 sample size from $n_2 = 10$ to $n_2 = 50$ ($n_2 = 10, 11, \ldots, 50$). This enabled simulation of the behaviour of the inference approaches assessed through an increase in sampling intensity in both auxiliary and field data, with sampling intensity (%)computed as $100 \bullet n/N_U$. A minimum sample size of 10 units was established with the aim of having a reasonably minimum dataset to fit the regression models. For each Monte Carlo simulation, the population mean was predicted ($\hat{\mu}^s$) using the respective estimator according to the inference approach applied, which implied refitting models using the Monte Carlo samples in those approaches using auxiliary data. This process was repeated numerous times n_{sim}, and the population mean (Eq. (14)) and its bias (Eq. (15)) and standard error (Eq. (16)) were then estimated as follows:

$$\hat{\mu}_{sim} = \frac{1}{n_{sim}} \sum_{s=1}^{n_{sim}} \hat{\mu}^s \tag{14}$$

$$\widehat{Bias}(\hat{\mu}_{sim}) = \frac{1}{n_{sim}} \sum_{s=1}^{n_{sim}} (\hat{\mu}^s - \mu) \tag{15}$$

$$\hat{se}_{\hat{\mu}_{sim}} = \sqrt{\frac{1}{n_{sim} - 1} \sum_{s=1}^{n_{sim}} (\hat{\mu}^s - \hat{\mu}_{sim})^2} \tag{16}$$

where s indicates the Monte Carlo samples, and n_{sim} is the number of simulations necessary for stabilization of $\hat{\mu}_{sim}$ and $\hat{se}_{\hat{\mu}_{sim}}$. n_{sim} was established as 10,000 according to previous works (McRoberts et al., 2022) and observed convergence of the estimated standard error (Fig. A.2). $\widehat{Bias}(\hat{\mu}_{sim})$ and $\hat{se}_{\hat{\mu}_{sim}}$ were estimated in relative terms as in Eqs. 17 and 18.

$$\widehat{Bias}(\hat{\mu}_{sim})(\%) = \frac{\widehat{Bias}(\hat{\mu}_{sim})}{\hat{\mu}_{sim}} \bullet 100 \tag{17}$$

$$\hat{se}_{\hat{\mu}_{sim}}(\%) = \frac{\hat{se}_{\hat{\mu}_{sim}}}{\hat{\mu}_{sim}} \bullet 100 \tag{18}$$

All of the previous estimates were computed for all the inference approaches evaluated, using the same notation as in Eqs. 14–18 but replacing the subscript *sim* by *EXP*, *REG*, *CMB* and 3p*HMB*, respectively. Finally, the relative efficiency (RE), given as the ratio between the estimated standard error for the EXP inference approach based on field data ($\hat{se}_{\hat{\mu}_{EXP}}$) and the other inference approaches ($\hat{se}_{\hat{\mu}_{EXP_{TLS}}}$, $\hat{se}_{\hat{\mu}_{REG}}$, $\hat{se}_{\hat{\mu}_{CMB}}$, $\hat{se}_{\hat{\mu}_{3pHMB}}$), was estimated as detailed in Eq. (19). The RE describes how much the number of field plots would need to be changed by the reference inference approach (EXP here) to obtain the same level of precision as with another estimator (EXP using TLS data, REG, CMB and 3pHMB in this study).

$$\begin{aligned} RE_{EXP_{TLS}} &= \frac{\hat{se}_{\hat{\mu}_{EXP}}}{\hat{se}_{\hat{\mu}_{EXP_{TLS}}}} \\ RE_{REG} &= \frac{\hat{se}_{\hat{\mu}_{EXP}}}{\hat{se}_{\hat{\mu}_{REG}}} \\ RE_{CMB} &= \frac{\hat{se}_{\hat{\mu}_{EXP}}}{\hat{se}_{\hat{\mu}_{CMB}}} \\ RE_{3pHMB} &= \frac{\hat{se}_{\hat{\mu}_{EXP}}}{\hat{se}_{\hat{\mu}_{3pHMB}}} \end{aligned} \tag{19}$$

4. Results

In this section, we have simplified the notation and removed the subscript *sim* when $\hat{\mu}_{sim}$, $\widehat{Bias}(\hat{\mu}_{sim})(\%)$ and $\hat{se}_{\hat{\mu}_{sim}}(\%)$ are cited. The Monte Carlo simulations showed that inference approaches incorporating remote sensing as auxiliary information consistently reduced the variability in the estimates of V, thereby also decreasing errors relative to those associated with design-based methods relying on a single source of information, either field or TLS data (Figs. A.3–4, Table 3). In addition, all approaches, except the CMB using the LPM to select the samples, were almost unbiased on average (Table 3), showing asymptotic behaviour, because the bias decreased as the sample size increases (Fig. 3). However, $\hat{\mu}_{EXP}$ was clearly negatively biased for most of the V estimates derived directly from TLS single-scans data, except for the estimators V.hn and V.hn.cov, with the latter showing the lowest level of bias (Fig. A.4, Table 3).

In the design-based approaches in which remotely sensed data were not used as auxiliary information, the error in EXP based on TLS estimates (V.hn.cov) was consistently slightly higher than the EXP approach using field data (Fig. 4a). Approaches using remote sensing data as auxiliary information yielded lower relative errors for almost all sampling intensities considered (Fig. 4b-c). However, the CMB approach yielded larger errors than any other for field sampling intensity lower than approximately 4 % (Fig. 4b). The mean errors, when no auxiliary remote sensing data were used, were even more than two times higher than 3pHMB and REG, with 11.27 % and 12.23 % for EXP with field and TLS data, respectively (Table 3). In terms of sampling intensity, both increasing the intensity of field sampling and increasing the intensity of TLS sampling reduced errors, as observed in approaches using partial coverage of TLS auxiliary data; the effect was more pronounced in REG inference approaches (Fig. 4c). As with the sample selection method, significant differences in errors between SRS and LPM were found for the lowest field sampling intensities in the case of the CMB inference

Table 3
Mean volume, bias and standard error estimates by inference approach and sample selection method.

Inference approach	TLS sampling intensity	$\widehat{\mu}$ (m^3 ha^{-1})		$\widehat{Bias}(\widehat{\mu})(\%)$		$\widehat{se}_{\widehat{\mu}}(\%)$	
		SRS	LPM	SRS	LPM	SRS	LPM
EXP (Field data)		254.45		−0.02		11.27	
EXP (TLS, V.tls)		209.39		−17.71		11.43	
EXP (TLS, V.sh)		222.53		−12.54		11.59	
EXP (TLS, V.hn)		252.27		−0.85		11.94	
EXP (TLS, V.hn.cov)		253.04		−0.55		12.23	
EXP (TLS, V.hr)		232.44		−8.65		11.96	
EXP (TLS, V.hr.cov)		240.03		−5.66		12.89	
	75 %	253.35	253.30	−0.44	−0.46	5.20	5.21
REG	50 %	253.39	253.37	−0.42	−0.43	5.67	5.67
	25 %	253.52	253.55	−0.37	−0.36	6.84	6.83
CMB		254.24	254.39	−0.24	−0.59	8.10	7.47
	75 %	252.97	253.34	−0.59	−0.44	5.60	4.95
3pHMB	50 %	252.92	253.33	−0.61	−0.44	5.71	4.98
	25 %	252.94	253.40	−0.60	−0.42	6.03	4.99

Values correspond to total averages considering all simulations of all sample sizes. Sample selection methods are simple random sampling (SRS) and local pivotal method (LPM).

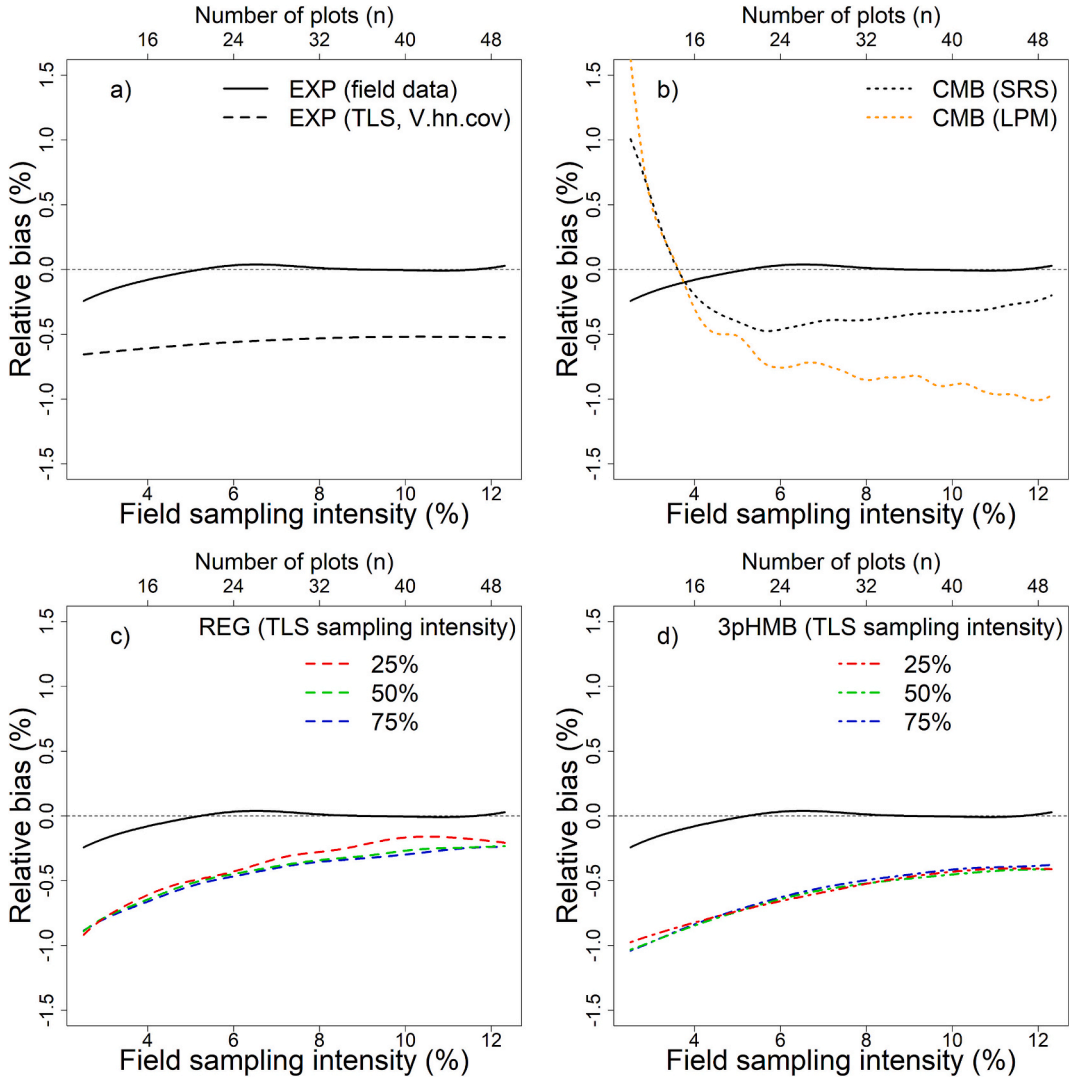

Fig. 3. Mean relative biases ($\widehat{Bias}(\widehat{\mu})(\%)$) obtained on the basis of 10,000 simulations per field sampling intensity and inference approach, fitted by nonparametric Nadaraya-Watson regression. In the case of inference approaches including TLS samples (REG and 3pHMB), 3 sampling intensities were considered (25 %, 50 %, 75 %). The figure shows cases in which 1st and 2nd phase samples were selected by SRS. Only in b a case in which the 1st phase sample was selected by LPM is shown.

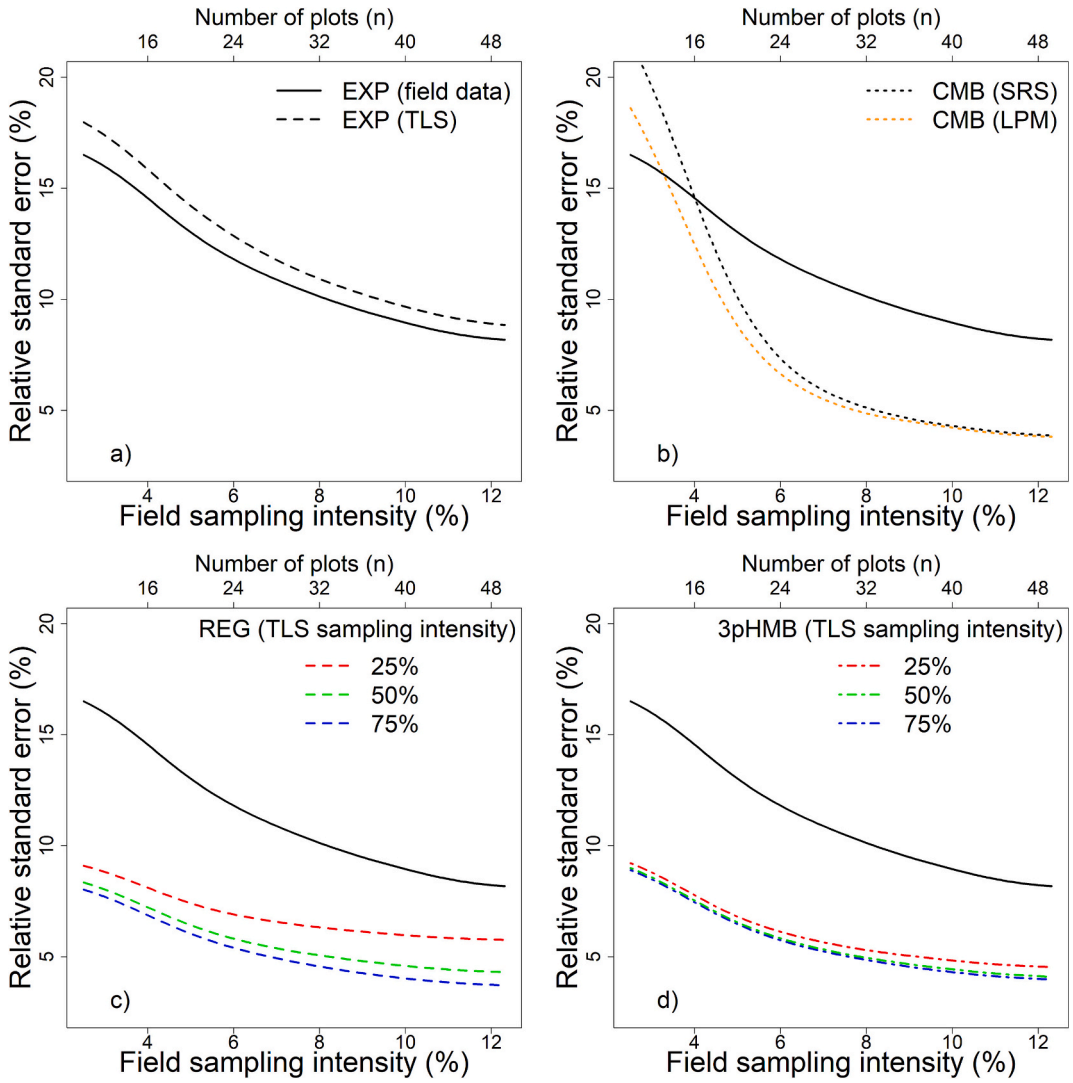

Fig. 4. Mean relative standard errors ($\widehat{se}_{\mu}(\%)$) obtained on the basis of 10,000 simulations per field sampling intensity and inference approach, fitted by nonparametric Nadaraya-Watson regression. In the case of inference approaches including TLS samples (REG and 3pHMB), 3 sampling intensities were considered (25 %, 50 %, 75 %). The figure shows cases in which 1st and 2nd phase samples were selected by SRS. Only in b is showed a case in which 1st phase sample were selected by LPM.

approach (Fig. 4b). Very similar errors were obtained in the case of the 3pHMB inference approach regardless of the TLS sampling intensity, while the REG approach yielded similar errors to those obtained with SRS (Fig. 5).

The relative efficiency of the EXP inference approach when directly using TLS *V* estimates (V.hn.cov) was slightly lower (0.90 approx.) and constant relative to the EXP approach using *V* estimates from field data (Fig. 6a). In situations with full coverage of auxiliary data, the CMB inference approach showed the greatest ability to increase the efficiency. This ranged from ratios as low as less than 1 for very low sampling intensities, to double the efficiency from a field sampling intensity of about 7 % (Fig. 6a). In addition, the sample selection method has an effect because LPM is more efficient for all field sampling intensities. As expected, for those designs using TLS partial coverage, sampling efficiency always decreased as TLS sampling intensity also decreased, particularly in the case of REG than 3pHMB (Fig. 6b-c). However, when LPM was used in the sample selection process, the latter inference approach yielded similar efficiency, always above 2, regardless of the TLS sampling intensity (Fig. 7b). Both REG and 3pHMB always showed higher efficiency than EXP for all field sampling intensities.

5. Discussion

As expected, the use of remote sensing (TLS and UAV-LiDAR devices) as a source of auxiliary data reduced the errors in *V* estimates in most cases, as observed for all inference approaches and most sampling sizes evaluated here. These findings are quite novel in relation to the use of ground-based LiDAR devices as a source of auxiliary data. However, this is consistent with the findings of many other studies using inference methodologies assisted by remotely sensed data, for example using non-parametric models with model-assisted and model-based inference approaches to estimate *V* among other forest attributes (Esteban et al., 2019). Some examples of the inference approaches assessed here can be found in previous studies, all of which used parametric models for predictions focused on regional and county level. Some examples include studies of model-assisted inferences using ALS strip data (Ene et al., 2012; Næsset et al., 2013), model-based inference with full coverage of ALS data (McRoberts et al., 2013), hierarchical model-assisted inference using ALS strip and wall-to-wall Landsat data (Saarela et al., 2015a) and hierarchical model-based inference using partial coverage of UAV-LiDAR and wall-to-wall Sentinel-2 data (Puliti et al., 2018). All remotely sensed data were used as auxiliary

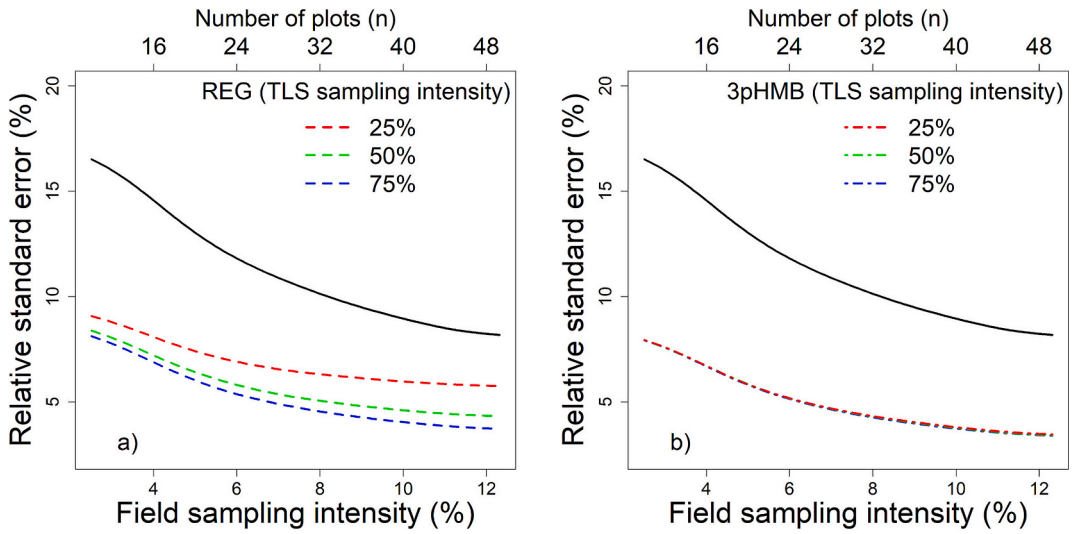

Fig. 5. Mean relative standard errors ($\widehat{se}_{\hat{\mu}}(\%)$) obtained on the basis of 10,000 simulations per field sampling intensity and inference approach, fitted by nonparametric Nadaraya-Watson regression. In the case of inference approaches including TLS samples (REG and 3pHMB), 3 sampling intensities were considered (25 %, 50 %, 75 %). The figure shows cases in which 1st and 2nd phase samples were selected by LPM.

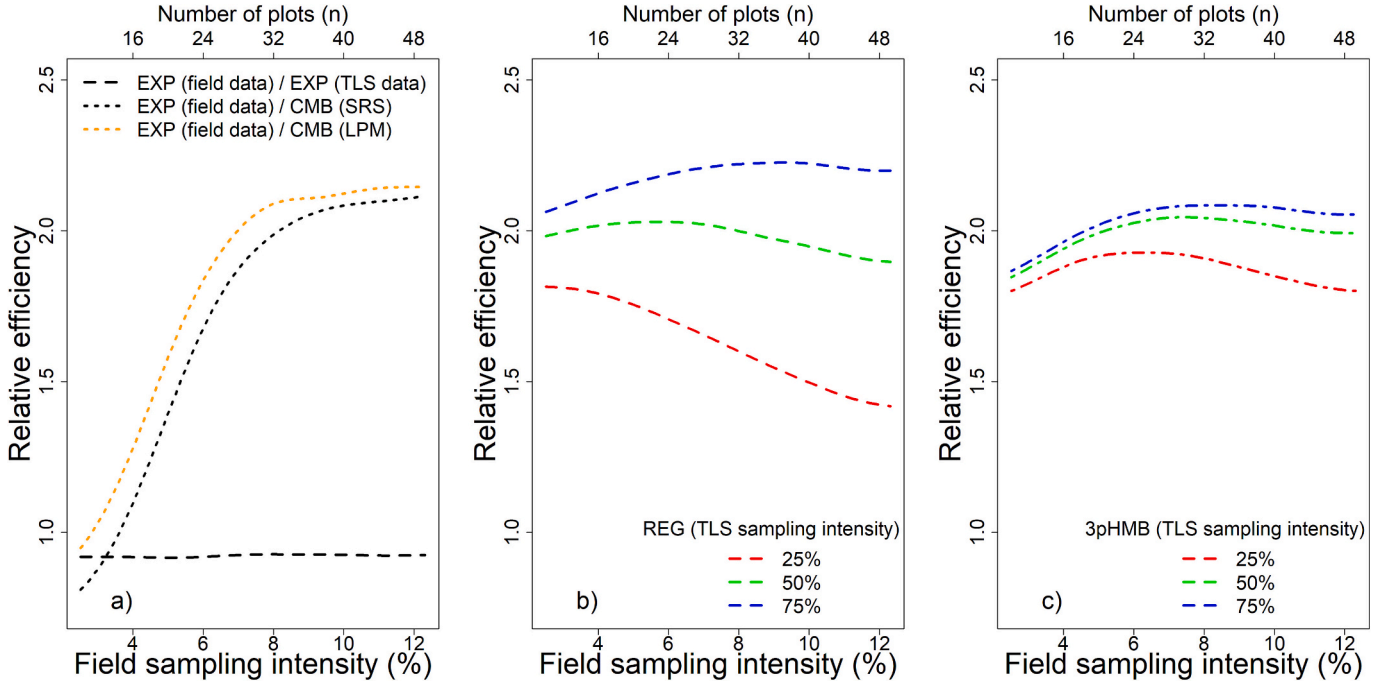

Fig. 6. Average relative efficiency, calculated as the ratio between $\widehat{se}_{\hat{\mu}_{EXP}}$ and $\widehat{se}_{\hat{\mu}_{EXP_{TLS}}}$, $\widehat{se}_{\hat{\mu}_{CMB}}$, $\widehat{se}_{\hat{\mu}_{REG}}$ and $\widehat{se}_{\hat{\mu}_{3pHMB}}$ over 10,000 simulations per field sampling intensity and inference approach, fitted by nonparametric Nadaraya-Watson regression. The main figure shows cases in which 1st and 2nd phase samples were selected by SRS.

information, together with field measured data which provided the true value of the estimated forest attribute (V). All of these studies also showed reductions in V estimation errors.

Focusing on EXP approaches, the best V estimates obtained from TLS single-scans corresponded to the V.hn.cov predictions based on distance sampling methodologies and applying the half-normal function expanded with *dbh* as a covariate to correct the probability of tree detection. This produced an approximately constant negative bias for the evaluated sample sizes of 0.55 % (approximately -1.40 m^3 ha^{-1}). However, this is not consistent with the observations of Astrup et al. (2014), who reported that the hazard-rate functions (V.hr and V.hr.cov estimates) led to greater precision than the half-normal detection functions, whereas the opposite was true in the present case. It would therefore be inappropriate to state that this approach would work in all situations, as the outcome will be influenced by other factors, such as forest structure. However, the results presented here indicate that occlusion correction methods can improve estimates as observed for basal area in angle-count (Lovell et al., 2011) and circular fixed area plots (Seidel and Ammer, 2014). For example, other methods used to correct for tree detection problems in estimating forest characteristics from single-scan TLS measurements yielded relative bias values of less than 3 % for estimating tree density and basal area (Kuronen et al., 2019). These findings indicate that calibration of these techniques may be a good compromise solution when using TLS in a single-scan configuration, as the lack of bias in the estimators is one of the desired properties in any type of inference approach. Nevertheless, the use of TLS as a pure

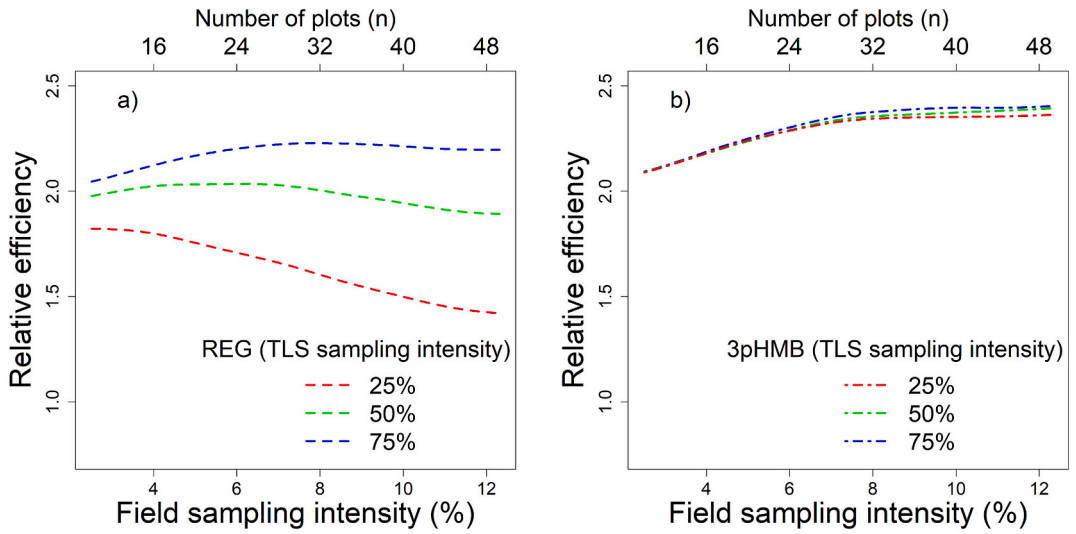

Fig. 7. Average relative efficiency, calculated as the ratio between $\widehat{se}_{\hat{\mu}_{EXP}}$ and $\widehat{se}_{\hat{\mu}_{REG}}$, $\widehat{se}_{\hat{\mu}_{3pHMB}}$ over 10,000 simulations per field sampling intensity and inference approach, fitted by nonparametric Nadaraya-Watson regression. The figure shows cases in which 1st and 2nd phase samples were selected by LPM.

EXP approach did not reduce estimation errors relative to the EXP approach based on field data, but rather increased them. This is due to increased variability in plot-level estimates caused by problems such as biased estimates of tree volume (Abegg et al., 2023; Vatandaşlar et al., 2023), and the shortfall in tree detection due to occlusions, among other factors (Liang et al., 2018). This may therefore be a disadvantage when using TLS as an operational tool in FI.

Regarding inference approaches using auxiliary data sources from remote sensing, the CMB approach was the only one that yielded larger errors than the EXP approaches for small field sampling intensities (approximately <4 %, < 16 plots). This may be due to poor model fit when the number of plots is small, as model performance is most important in these inference methods (Gregoire, 1998). This finding is consistent with those of a previous study conducted under relatively similar conditions (40 ha of *Pinus radiata* plantation), in which the gain in accuracy in the CMB approach using UAV-LiDAR and 30 field plots (4.5 % field sampling intensity) was relatively small relative to that in the EXP approach based on field data (Puliti et al., 2020). The study authors (*op.cit.*) attributed the small difference to the relative homogeneous nature of the sample stand and relative larger sampling intensity of field data. However, for a similar number of field plots in this work, the error in the CMB approach was also smaller than in the EXP approach. Therefore, both the field sampling intensity and the number of field plots were important for reducing errors. Only linear regression models with up to 3 explanatory variables were evaluated here, while other studies have used other types of regression such as power regression models (Guerra-Hernández et al., 2022). Therefore, the conclusions drawn from this case study should be considered with caution, because, as previously mentioned, modelling is a fundamental part of model-based inference. By contrast, the number of field plots used to fit the models was more decisive when UAV-LiDAR data were used as the only auxiliary information, since in the case of REG and 3pHMB inference approaches, errors were always lower than in EXP, even for the lowest field sampling intensities. In addition, the first-stage sample size was more important to increase precision in the REG inference, as observed by McRoberts et al. (2024), who showed that the error was reduced by approximately 16 % in biomass estimates by increasing the first-stage intensity from 25 to 1000 plots. The accuracy was similar to that obtained in the 3pHMB inference approach when SRS was used, where the second phase (that of TLS data) was more decisive in reducing errors. However, this effect was less pronounced than in the REG approach. This finding is consistent with those of Saarela et al. (2015a), who reported that in hierarchical model-assisted approaches involving wall-to-wall data sources, the ability to reduce errors by increasing sampling intensity of the second phase (ALS LiDAR strips in that case) was lower than in the REG approaches.

The use of the auxiliary information to improve the estimates (probability-proportional-to-size sampling in that case) did not yield a significant reduction in errors in most cases, unlike in Saarela et al. (2015a). This may have been expected, as the area is small and too homogeneous to show the true benefits of this approach. However, the LPM proved to be useful for reducing errors when wall-to-wall UAV-LiDAR auxiliary data were used. This was observed in CMB and with low field data sampling intensities, where the LPM did yield a reduction in errors. Nevertheless, estimates obtained with this approach were slightly biased without showing asymptotic behaviour. This may be due to overfitting issues, which can tend to produce biased estimated population means (Cosenza et al., 2024). The 3pHMB approach also yielded slightly smaller errors when the LPM was applied, and these were very similar regardless of the sampling intensity of the second phase. TLS is therefore more competitive in terms of error reduction when SRS is applied probably due to higher correlations between the response variable *V* and auxiliary information as potential explanatory variables (e.g. V.tls). The fitted models with TLS auxiliary data could thus have smaller errors both within and outside the range of the explanatory variables (i.e. providing more generalist predictions), leading to fewer errors in predictions, as model performance was again the most important in these inference approaches (Gregoire, 1998). Ground-based LiDAR techniques therefore clearly have an advantage of over airborne LiDAR, as traditional design-based sampling, which distributes sampling units without support from remotely sensed information, would still work reasonably well for small field samples. This also explains the very low margin for reducing errors with a certain field data sample size large enough to fit good models, because the model error contributes the same to the total variance regardless of the size of the auxiliary data sample (Saarela et al., 2015b).

In terms of relative efficiency (RE), all approaches using remotely sensed data aimed to reduce the intensity of field sampling (usually the most costly and time-consuming phase) at the expense of increasing the intensity of remote sensing sampling (usually the least time-consuming phase). This particularly applied to low field sampling intensities, as currently used in FIs (Lister et al., 2020) and was especially notable in the case of CMB, where small increases in field sampling intensity led to large increases in RE until they plateaued slightly above 2. However, the RE was not as high as in other studies, in which RE values of 2.5–8 were reached (Ene et al., 2012; Næsset et al., 2013; Puliti et al., 2017).

According to Puliti et al. (2020), the modest gains in RE probably reflect the relatively homogenous nature of the study plot. Although the REG and 3pHMB approaches already yielded higher RE with low sampling intensities, it barely increased, but rather decreased as field sampling intensity increased. This was more pronounced for small TLS sampling intensities, and even more so for REG than for 3pHMB. Focusing on the use of the LPM for sample selection, the RE improved slightly in those cases using wall-to-wall UAV-LiDAR (CMB and 3pHMB). This finding suggests that use of LPM can improve estimates when the auxiliary data source belongs to UAV-LiDAR, as already demonstrated with ALS data (Goodbody et al., 2023).

Although similar future studies may focus on replacing the field data phase with data obtained by TLS multi-scan or MLS in order to reduce tree occlusions issues (Bauwens et al., 2016; Liang et al., 2018), it was demonstrated that the source of error associated with sampling would be similar to or even higher than in the conventional EXP approach based solely on field data. Nevertheless, other sources of error, such as biased volume estimates produced by allometric models, may be reduced by using TLS as demonstrated for biomass estimates (Stovall et al., 2023). However, young trees are scarcely detected by ground-based technologies (Liang et al., 2018), thus producing biased estimates with the current algorithms and devices (Abegg et al., 2023). The use of close-range LiDAR devices as sources of auxiliary data can cope with this problem, even allowing the estimation of attributes for very young stand stages, hence improving forest management and planning overall. On the basis of the findings, the present study therefore represents a step towards the use of close-range LiDAR technologies in FIs at stand level, exploring for the first time the use of ground-based technologies in an area-based approach. Moreover, unlike other studies in which the entire population is unknown or simulated, the entire reference population was known in this study. This is important for application of the findings to similar cases.

6. Conclusions

The inference approaches based on auxiliary information data usually reduced errors in *V* estimates below those based on a single source of information (EXP approach), both for field data and TLS data. In this regard, the novel use of TLS auxiliary data in the REG and 3pHMB inference approaches improved the *V* estimates, leading to smaller estimation errors. On the one hand, the CMB approach using UAV-LiDAR data required a higher field sampling intensity to increase the efficiency relative to EXP approaches. On the other hand, REG and 3pHMB inference approaches were more efficient than EXP approaches, even at low field sampling intensities. All of these findings suggest that close-range LiDAR devices show some potential as stand-level measurement instruments, at least in terms of error reduction. However, the findings cannot be generalized to populations that are very different from those considered in this case study. Transfer of these techniques to realistic situations may play an important role in operationalizing the use of close-range LiDAR devices in FIs, specifically ground-based devices, which have been a recent addition to forest sampling. As has been the case with other remote sensing methods, the next step should focus on evaluating the universality of these methods both by replicating them in other situations and by improving the methods applied.

CRediT authorship contribution statement

Juan Alberto Molina-Valero: Writing – original draft, Software, Project administration, Methodology, Investigation, Funding acquisition, Formal analysis, Data curation, Conceptualization. **Rorai Pereira Martins-Neto:** Writing – review & editing, Software, Data curation. **Adela Martínez-Calvo:** Writing – original draft, Software. **Joel Rodríguez-Ruiz:** Writing – original draft, Data curation. **Peter Surový:** Writing – original draft, Resources. **Anika Seppelt:** Writing – original draft, Software, Data curation. **César Pérez-Cruzado:** Writing – original draft, Supervision, Resources, Project administration, Methodology, Funding acquisition, Conceptualization.

Declaration of competing interest

The authors declare that they have no known competing financial interests or personal relationships that could have appeared to influence the work reported in this paper.

Acknowledgements

Funding: This work was supported by the Galician Regional Government [ED431F 2020/02] and the Spanish Ministry of Science and Innovation [PID2020-119204RB-C22]. JAMV was supported by the Postdoctoral Fellow "Becas Fundación Ramón Areces para Estudios Postdoctorales" [BEVP35A7109] and the MSCA-COFUND Fellow within the framework of the project "Central Bohemian Mobility Programme for Excellence in Research, Innovation and Technology" [GA 101081195-MERIT]; AMC was supported by the Galician Regional Government within the framework of the agreement "Development of the Galician Continuous Forest Inventory" [2020-CP031]; JRR was supported by the predoctoral contract Campus Terra-USC 2022; and CPC was supported by the Spanish Ministry of Science and Innovation [RYC2018-024939-I].

The authors thank Diego Lombardero Barrera, Eduardo Seijo De Bernardo, Mario López Fernández and Óscar López Álvarez for help with fieldwork. The authors are also grateful for the comments made by anonymous reviewers, which helped to improve the quality of the paper. The authors also thank Christine Francis for her assistance with the language usage and Vítězslav Moudrý for reviewing the manuscript.

Appendix A. Appendix

Table A.1
Variables obtained with *FORTLS*.

Variables	Description
N.tls	Stand density (*N*, trees ha^{-1}).
G.tls	Stand basal area (*G*, $m^2\ ha^{-1}$).
V.tls	Stand timber volume (*V*, $m^3\ ha^{-1}$).
V.com	Stand timber volume up to a limiting diameter (V_c, $m^3\ ha^{-1}$).
h.com.tls	Stand length of logs up to a limiting diameter (h_c, $m\ ha^{-1}$).
N.hn*, N.hr*, N.hn.cov*, N.hr.cov*, G.hn*, G.hr*, G.hn.cov*, G.hr.cov*, V.hn*, V.hr*, V.hn.cov*, V.hr.cov**	*N*, *G* and *V* with occlusion corrections based on distance sampling methodologies. In the case of V_c and h_c, the ".com" ending will be added (e.g. V.com.hn).

(*continued on next page*)

Table A.1 (*continued*)

Variables	Description
N.sh*, G.sh*, V.sh*	*N*, *G* and *V* with correction of the shadowing effect. In the case of V_c and h_c, the ".com" ending will be added (e.g. V.com.sh).
N.pam**, G.pam**, V.pam**	*N*, *G* and *V* with occlusion correction based on a Poisson attenuation model. In the case of V_c and h_c, the ".com" ending will be added (e.g. V.com.pam).
d.tls, dg.tls, dgeom.tls, dharm.tls	Stand mean *dbh* (cm), using arithmetic ($\bar{d}$), quadratic (d_g), geometric, and harmonic means, respectively.
h.tls, hg.tls, hgeom.tls, hharm.tls	Stand mean height (*h*, m), using arithmetic, quadratic, geometric, and harmonic means, respectively.
d.0.tls, dg.0.tls, dgeom.0.tls, dharm.0.tls	Stand dominant mean *dbh*(D_0, cm), using arithmetic, quadratic, geometric, and harmonic means, respectively.
h.0.tls, hg.0.tls, hgeom.0.tls, hharm.0.tls	Stand dominant mean *h* (H_0, m), using arithmetic, quadratic, geometric, and harmonic means, respectively.

* Variables only estimated for circular fixed area and k-tree plot design.
** Variables only estimated for angle-count plot design.

Table A.2
Metrics obtained with *FORTLS*.

Metrics	Description
n.pts, n.pts.est, n.pts.red, n.pts.red.est	Number of points and estimated number of points corresponding to normal sections slices (1.3 ± 0.05 m) of trees in the original point cloud (n.pts and n.pts.est, respectively); and number of points and estimated number of points corresponding to normal sections slices of trees in the reduced point cloud (n.pts.red and n.pts.red.est, respectively).
P01, …, P99	Percentiles (m) of height (z coordinate) distribution.
mean.arit.z/rho/r, mean.qua.z/rho/r, mean.geom.z/rho/r, mean.harm.z/rho/r, median.z/rho/r, mode.z/rho/r	Central tendency statistics of the coordinates z, ρ (rho, horizontal distance) and r (radial distance or Euclidean distance to TLS): arithmetic, quadratic, geometric and harmonic means; median; and mode, respectively.
var.z/rho/r, sd.z/rho/r, cv.z/rho/r, d.z/rho/r, id.z/rho/r, max.z/rho/r, min.z/rho/r	Dispersion statistics of the coordinates z, ρ and r: variance, standard deviation, coefficient of variation, range, interquartile range, maximum, and minimum, respectively.
skewness.z/rho/r, kurtosis.z/rho/r	Coefficients of skewness and kurtosis of the distribution of z, ρ and r coordinates, respectively.
L2.z/rho/r, L3.z/rho/r, L4.z/rho/r, L.skewness.z/rho/r, L.kurtosis.z/rho/r, L.CV.z/rho/r	L-moments of order 2 (λ_2), 3 (λ_3) and 4 (λ_4) of the of z, ρ and r coordinates, respectively. L-moments ratios of order 2 (τ, L-CV, coefficient of L-variation $= \lambda_2/\lambda_1$), 3 (τ_3, L-skewness $= \lambda_3/\lambda_2$) and 4 (τ_4, L-kurtosis $= \lambda_4/\lambda_2$) of the of z, ρ and r coordinates, respectively.
median.a.dz/rho/r, mode.a.d.z/rho/r	Median of the absolute deviations from the overall median; and mode of the absolute deviations from the overall mode, respectively.
p.a.mean.z/rho/r, p.a.mode.z/rho/r, p.a.2 m	Percentage of points above arithmetic mean, mode (coordinates z, ρ and r) and 2 m (z).
p.b.mean.z/rho/r, p.b.mode.z/rho/r, p.b.2 m	Percentage of points below arithmetic mean, mode (coordinates z, ρ and r) and 2 m (z).
weibull.b.z/rho/r, weibull.c.z/rho/r	Scale and shape parameters, respectively, for Weibull distribution fitted for the coordinates z, ρ and r.
CRR.z/rho/r	Canopy relief ratio (arithmetic mean / maximum) for the coordinates z, ρ and r.

Table A.3
UAV-LiDAR metrics extracted by plot*.

Metrics	Description
zmax, zmean, zmin	Maximum, mean and minimum height.
zsd, zcv, zskew, zkurt, zentropy	Standard deviation, coefficient of variation, skewness, kurtosis, and entropy of height distributions.
zq_x	Xth percentile (1, 5, 10, 15, 20, 25, 30, 35, 40, 45, 50, 55, 60, 65, 70, 75, 80, 85, 90, 95, 99) of height distribution.
pzabovemean, pzabove2, pzabove5	Percentage of returns above the mean height, 2 m and 5 m.
zi_{qr}	Interquartile distance.
zMADmean, zMADmedian	Mean absolute deviation from the mean and the median height.
CRR	Canopy relief ratio $\left(\frac{zmean - zmin}{zmax - zmin}\right)$.
VCI	Vertical complexity index (van Ewijk et al., 2011).
$zpcum_x$	Cumulative percentage of return in the Xth layer (1 to 9) with f(z) the probability distribution of heights.
L1, L2, L3, L4, Lskew, Lkurt. Lcv	L-moments, skewness, kurtosis and coefficient of variation of L-moment.

(*continued on next page*)

Table A.3 (*continued*)

Metrics	Description
LAI	Leaf area index.
LAD_max, LAD_mean, LAD_min, LAD_cv	Leaf area density maximum, mean, minimum and coefficient of variation.
pz_below_0, pz_0.0.15, pz_0.15.2, pz_2.5, pz_5.10, pz_10.20, pz_20.30, pz_above_30	Interval metrics - proportion of returns between specified elevation intervals. Default intervals are 0, 0.15, 2, 5, 10, 20 and 30.
OpenGapSpace, ClosedGapSpace, Euphotic, Oligophotic	Canopy volume classes (Lefsky et al., 1999).
pFirst, pIntermediate, pLast, pSingle, pMultiple	Percentage of returns by echo types (First, Intermediate, Last, and Single, Multiple).

* Adapted from (McGaughey, 2019; Tompalski and Goodbody, 2021).

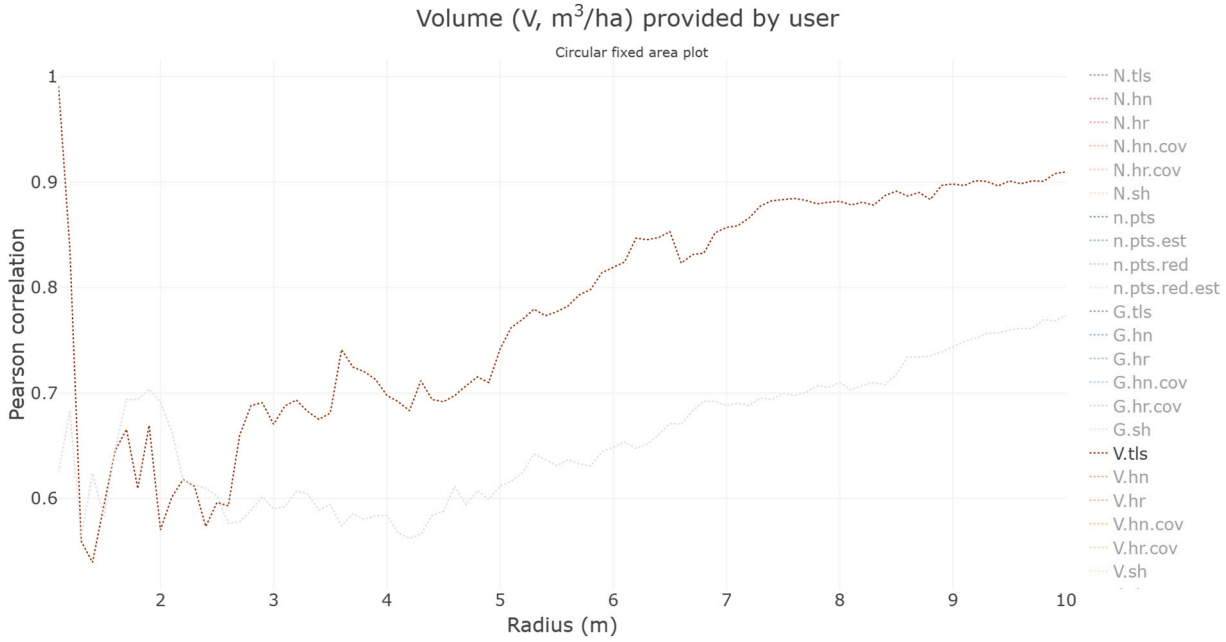

Fig. A.1. Line graph showing the correlations between *V* and V.tls (brown line) and *V* and percentile 95 (grey line), derived from simulated TLS and field plots, for circular fixed are plot design according to regular 0.1 m increments in radius. (For interpretation of the references to colour in this figure legend, the reader is referred to the web version of this article.)

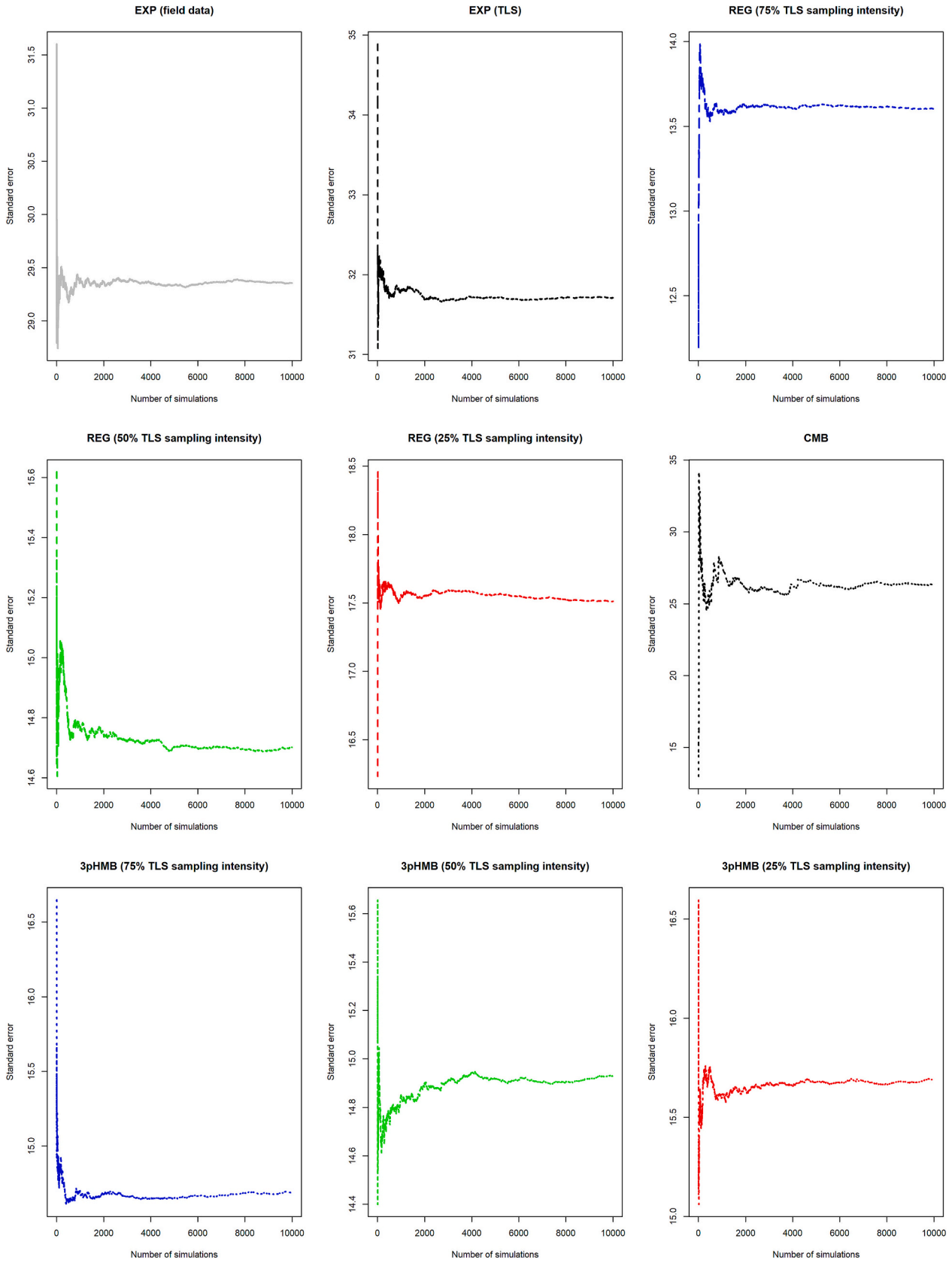

Fig. A.2. Convergence of the estimated standard error over 10,000 simulations per sample size. EXP (TLS) refers to the V.tls variable (see Table A.1).

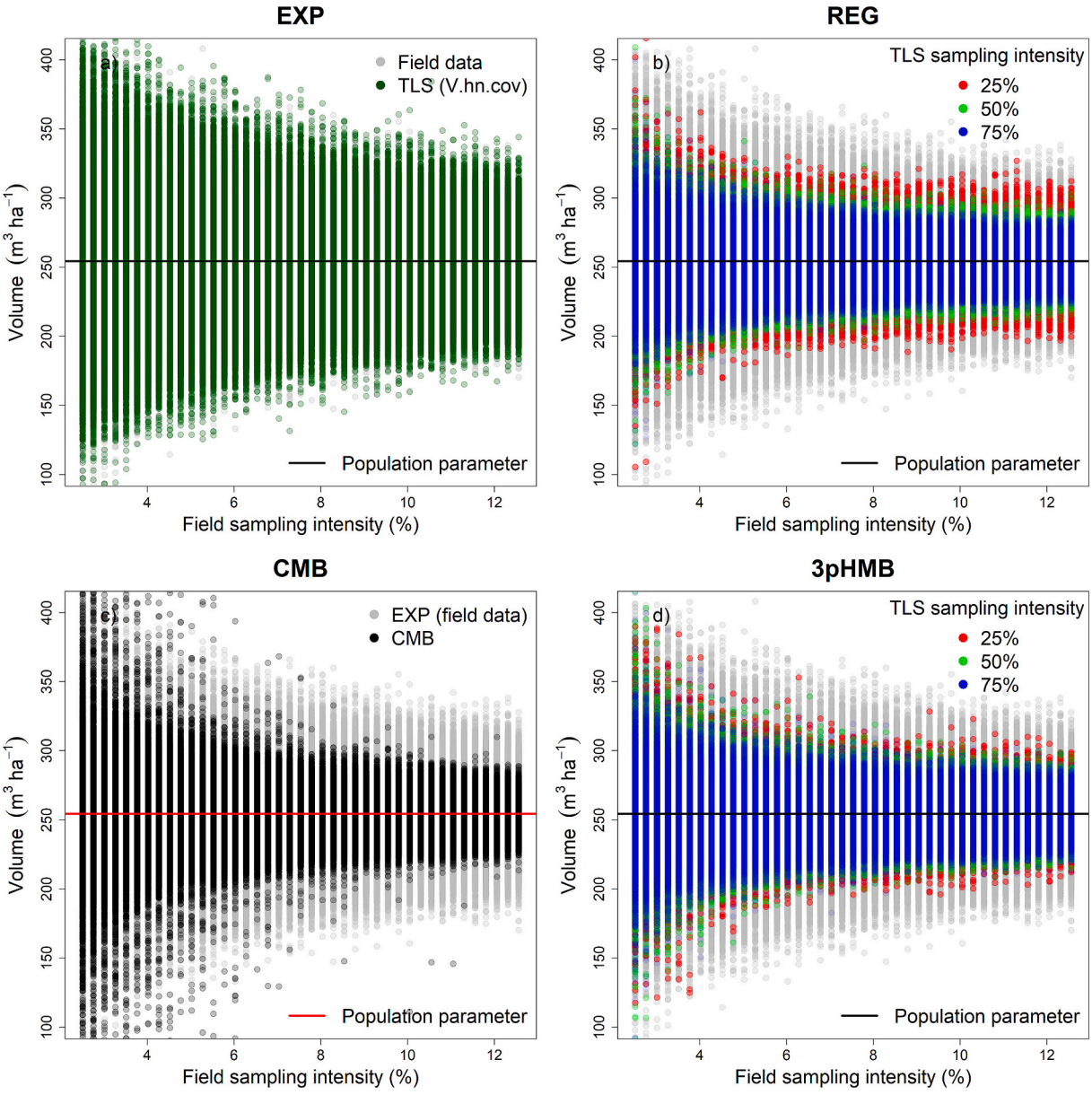

Fig. A.3. Mean volume estimates ($\hat{\mu}$) obtained on the basis of 10,000 simulations per field sampling intensity and inference approach. In the case of inference approaches including TLS samples (REG and 3pHMB), 3 sampling intensities were considered (25 %, 50 %, 75 %). This figure shows cases in which 1st and 2nd phase samples were selected by simple random sampling (SRS).

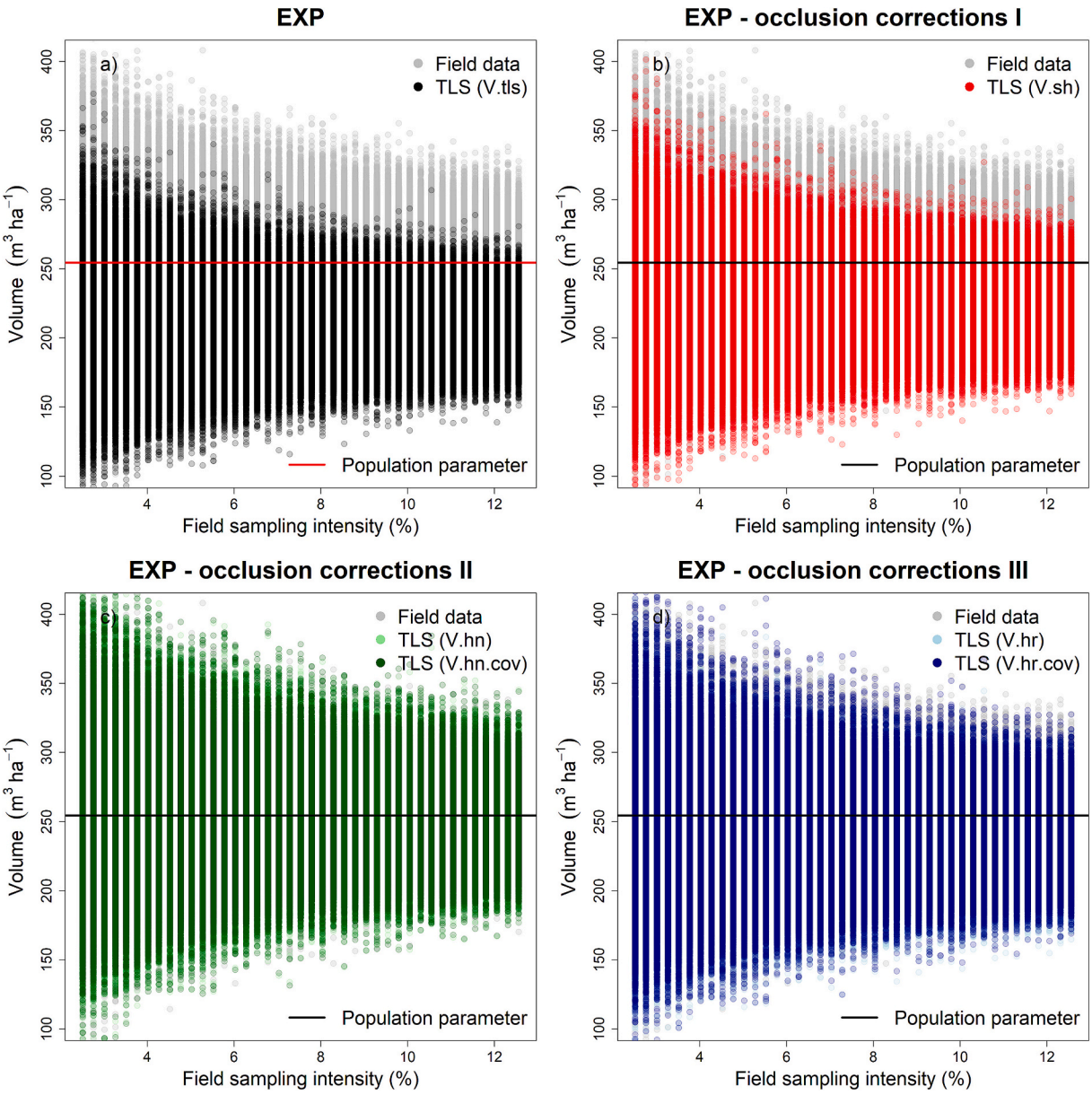

Fig. A.4. Mean volume estimates ($\widehat{\mu}$) obtained in the EXP approach on the basis of 10,000 simulations per field sampling intensity and different *V* estimates, such as $\widehat{\mu}$ based on field data (a, b, c and d); $\widehat{\mu}$ based on TLS data (V.tls, a); $\widehat{\mu}$ based on TLS data correcting the shadowing effect (V.sh, b); $\widehat{\mu}$ based on TLS data implementing distance sampling methods using the half-normal function (V.hn and V.hn.cov, c); and $\widehat{\mu}$ based on TLS data implementing distance sampling methods using the hazard-rate function (V.hr and V.hr.cov, d).

Data availability

The authors do not have permission to share data.

References

Abegg, M., Bösch, R., Kükenbrink, D., Morsdorf, F., 2023. Tree volume estimation with terrestrial laser scanning—testing for bias in a 3D virtual environment. Agric. For. Meteorol. 331, 109348. https://doi.org/10.1016/j.agrformet.2023.109348.

Andersen, H.E., Strunk, J., Temesgen, H., 2011. Using airborne light detection and ranging as a sampling tool for estimating forest biomass resources in the upper Tanana Valley of interior Alaska. West. J. Appl. For. 26 (4), 157–164. https://doi.org/10.1093/WJAF/26.4.157.

Astrup, R., Ducey, M.J., Granhus, A., Ritter, T., von Lüpke, N., 2014. Approaches for estimating stand-level volume using terrestrial laser scanning in a single-scan mode. Can. J. For. Res. 44 (6), 666–676. https://doi.org/10.1139/cjfr-2013-0535.

Bauwens, S., Bartholomeus, H., Calders, K., Lejeune, P., 2016. Forest inventory with terrestrial LiDAR: a comparison of static and hand-held mobile laser scanning. Forests 7 (6), 127. https://doi.org/10.3390/f7060127.

Breidenbach, J., McRoberts, R.E., Astrup, R., 2016. Empirical coverage of model-based variance estimators for remote sensing assisted estimation of stand-level timber volume. Remote Sens. Environ. 173, 274–281. https://doi.org/10.1016/j.rse.2015.07.026.

Buckland, S.T., Anderson, D.R., Burnham, K.P., Laake, J.L., Borchers, D.L., Thomas, L., 2001. Introduction to Distance Sampling: Estimating Abundance of Biological Populations. Oxford University Press.

Calders, K., Adams, J., Armston, J., Bartholomeus, H., Bauwens, S., Bentley, L.P., Chave, J., Danson, F.M., Demol, M., Disney, M., Gaulton, R., Krishna Moorthy, S.M., Levick, S.R., Saarinen, N., Schaaf, C., Stovall, A., Terryn, L., Wilkes, P., Verbeeck, H., 2020. Terrestrial laser scanning in forest ecology: expanding the horizon. Remote Sens. Environ. 251, 112102. https://doi.org/10.1016/J.RSE.2020.112102.

Cassel, C.-M., Särndal, C.-E., Wretman, J.H., 1977. Foundations of Inference in Survey Sampling. Wiley.

Cochran, W.G., 1977. Sampling techniques. John Wiley& Sons.

Coops, N.C., Tompalski, P., Goodbody, T.R.H., Queinnec, M., Luther, J.E., Bolton, D.K., White, J.C., Wulder, M.A., van Lier, O.R., Hermosilla, T., 2021. Modelling lidar-

derived estimates of forest attributes over space and time: a review of approaches and future trends. Remote Sens. Environ. 260, 112477. https://doi.org/10.1016/J.RSE.2021.112477.
Coops, N.C., Tompalski, P., Goodbody, T.R.H., Achim, A., Mulverhill, C., 2023. Framework for near real-time forest inventory using multi source remote sensing data. Forestr.: Int. J. Forest Res. 96 (1), 1–19. https://doi.org/10.1093/FORESTRY/CPAC015.
Corona, P., Fattorini, L., Franceschi, S., Scrinzi, G., Torresan, C., 2014. Estimation of standing wood volume in forest compartments by exploiting airborne laser scanning information: model-based, design-based, and hybrid perspectives. Can. J. For. Res. 44 (11), 1303–1311. https://doi.org/10.1139/CJFR-2014-0203.
Cosenza, D.N., Saarela, S., Strunk, J., Korhonen, L., Maltamo, M., Packalen, P., 2024. Effects of model-overfit on model-assisted forest inventory in boreal forests with remote sensing data. Forestr.: Int. J. Forest Res. cpae055. https://doi.org/10.1093/forestry/cpae055.
Dassot, M., Constant, T., Fournier, M., 2011. The use of terrestrial LiDAR technology in forest science: application fields, benefits and challenges. Ann. For. Sci. 68 (5), 959–974. https://doi.org/10.1007/S13595-011-0102-2.
Deville, J.C., Tillé, Y., 1998. Unequal probability sampling without replacement through a splitting method. Biometrika 85 (1), 89–101. https://doi.org/10.1093/BIOMET/85.1.89.
Diéguez-Aranda, U., Rojo Alboreca, A., Castedo-Dorado, F., Álvarez González, J.G., Barrio-Anta, M., Crecente-Campo, F., González González, J.M., Pérez-Cruzado, C., Rodríguez Soalleiro, R., López-Sánchez, C.A., Balboa-Murias, M.Á., Gorgoso Varela, J.J., Sánchez Rodríguez, F., 2009. Herramientas selvícolas para la gestión forestal sostenible en Galicia. Dirección Xeral de Montes, Consellería do Medio Rural, Xunta de Galicia.
Dubayah, R.O., Drake, J.B., 2000. Lidar Remote Sensing for Forestry. J. For. 98 (6), 44–46. https://doi.org/10.1093/JOF/98.6.44.
Ducey, M.J., Astrup, R., 2013. Adjusting for nondetection in forest inventories derived from terrestrial laser scanning. Can. J. Remote. Sens. 39 (5), 410–425. https://doi.org/10.5589/m13-048.
Ene, L.T., Næsset, E., Gobakken, T., Gregoire, T.G., Ståhl, G., Nelson, R., 2012. Assessing the accuracy of regional LiDAR-based biomass estimation using a simulation approach. Remote Sens. Environ. 123, 579–592. https://doi.org/10.1016/J.RSE.2012.04.017.
Esteban, J., McRoberts, R.E., Fernández-Landa, A., Tomé, J.L., Næsset, E., 2019. Estimating forest volume and biomass and their changes using random forests and remotely sensed data. Remote Sens. 11 (16), 1944. https://doi.org/10.3390/RS11161944.
Fassnacht, F.E., White, J.C., Wulder, M.A., Naesset, E., 2023. Remote sensing in forestry: current challenges, considerations and directions. Forestr.: Int. J. Forest Res. 2023, 1–27. https://doi.org/10.1093/FORESTRY/CPAD024.
Firth, D., Bennett, K.E., 1998. Robust models in probability sampling. J. R. Stat. Soc. Ser. B Stat Methodol. 60 (1), 3–21. https://doi.org/10.1111/1467-9868.00105.
Goodbody, T.R.H., Coops, N.C., Senf, C., Seidl, R., 2023. Airborne laser scanning to optimize the sampling efficiency of a forest management inventory in south-eastern Germany. Ecol. Indic. 157, 111281. https://doi.org/10.1016/j.ecolind.2023.111281.
Grafström, A., Schelin, L., 2014. How to select representative samples. Scand. J. Stat. 41 (2), 277–290. https://doi.org/10.1111/SJOS.12016.
Grafström, A., Lundström, N.L.P., Schelin, L., 2012. Spatially balanced sampling through the pivotal method. Biometrics 68 (2), 514–520. https://doi.org/10.1111/J.1541-0420.2011.01699.X.
Grafström, A., Saarela, S., Ene, L.T., 2014. Efficient sampling strategies for forest inventories by spreading the sample in auxiliary space. Can. J. For. Res. 44 (10), 1156–1164. https://doi.org/10.1139/CJFR-2014-0202.
Grafström, A., Prentius, W., Lisic, J.. BalancedSampling: Balanced and Spatially Balanced Sampling. https://CRAN.R-project.org/package=BalancedSampling.
Gregoire, T.G., 1998. Design-based and model-based inference in survey sampling: appreciating the difference. Can. J. For. Res. 28 (10), 1429–1447. https://doi.org/10.1139/x98-166.
Gregoire, T.G., Ståhl, G., Næsset, E., Gobakken, T., Nelson, R., Holm, S., 2011. Model-assisted estimation of biomass in a LiDAR sample survey in Hedmark County, Norway. Can. J. For. Res. 41 (1), 83–95. https://doi.org/10.1139/X10-195.
Guerra-Hernández, J., Botequim, B., Bujan, S., Jurado-Varela, A., Molina-Valero, J.A., Martínez-Calvo, A., Pérez-Cruzado, C., 2022. Interpreting the uncertainty of model-based and design-based estimation in downscaling estimates from NFI data: a case-study in Extremadura (Spain). GISci. & Remote Sens. 59 (1), 686–704. https://doi.org/10.1080/15481603.2022.2051383.
Kangas, A., Astrup, R., Breidenbach, J., Fridman, J., Gobakken, T., Korhonen, K.T., Maltamo, M., Nilsson, M., Nord-Larsen, T., Næsset, E., Olsson, H., 2018. Remote sensing and forest inventories in Nordic countries–roadmap for the future. Scand. J. For. Res. 33 (4), 397–412. https://doi.org/10.1080/02827581.2017.1416666.
Krok, G., Kraszewski, B., Stereńczak, K., 2020. Application of Terrestrial Laser Scanning in Forest Inventory–An Overview of Selected Issues. Leśne Prace Badawcze / Forest Research Papers 81 (4), 175–194. https://doi.org/10.2478/frp-2020-0021.
Kuronen, M., Henttonen, H.M., Myllymäki, M., 2019. Correcting for nondetection in estimating forest characteristics from single-scan terrestrial laser measurements. Can. J. For. Res. 49 (1), 96–103. https://doi.org/10.1139/cjfr-2018-0072.
Kuželka, K., Marušák, R., Surový, P., 2022. Inventory of close-to-nature forest stands using terrestrial mobile laser scanning. Int. J. Appl. Earth Obs. Geoinf. 115, 103104. https://doi.org/10.1016/J.JAG.2022.103104.
Liang, X., Kankare, V., Hyyppä, J., Wang, Y., Kukko, A., Haggrén, H., Yu, X., Kaartinen, H., Jaakkola, A., Guan, F., Holopainen, M., Vastaranta, M., 2016. Terrestrial laser scanning in forest inventories. ISPRS J. Photogramm. Remote Sens. 115, 63–77. https://doi.org/10.1016/J.ISPRSJPRS.2016.01.006.
Lefsky, M.A., Cohen, W.B., Acker, S.A., Parker, G.G., Spies, T.A., Harding, D., 1999. Lidar remote sensing of the canopy structure and biophysical properties of Douglas-fir western hemlock forests. Remote Sens. Environ. 70 (3), 339–361. https://doi.org/10.1016/S0034-4257(99)00052-8.
Liang, X., Hyyppä, J., Kaartinen, H., Lehtomäki, M., Pyörälä, J., Pfeifer, N., Holopainen, M., Brolly, G., Francesco, P., Hackenberg, J., Huang, H., Jo, H.W., Katoh, M., Liu, L., Mokroš, M., Morel, J., Olofsson, K., Poveda-Lopez, J., Trochta, J., Wang, Y., 2018. International benchmarking of terrestrial laser scanning approaches for forest inventories. ISPRS J. Photogramm. Remote Sens. 144, 137–179. https://doi.org/10.1016/J.ISPRSJPRS.2018.06.021.
Lister, A.J., Andersen, H., Frescino, T., Gatziolis, D., Healey, S., Heath, L.S., Liknes, G.C., McRoberts, R., Moisen, G.G., Nelson, M., Riemann, R., Schleeweis, K., Schroeder, T. A., Westfall, J., Wilson, B.T., 2020. Use of remote sensing data to improve the efficiency of national forest inventories: a case study from the United States national forest inventory. Forests 11 (12), 1364. https://doi.org/10.3390/f11121364.
Lovell, J.L., Jupp, D.L.B., Culvenor, D.S., Coops, N.C., 2003. Using airborne and ground-based ranging lidar to measure canopy structure in Australian forests. Can. J. Remote. Sens. 29 (5), 607–622. https://doi.org/10.5589/M03-026.
Lovell, J.L., Jupp, D.L.B., Newnham, G.J., Culvenor, D.S., 2011. Measuring tree stem diameters using intensity profiles from ground-based scanning lidar from a fixed viewpoint. ISPRS J. Photogramm. Remote Sens. 66 (1), 46–55. https://doi.org/10.1016/j.isprsjprs.2010.08.006.
Luck, L., Kaestli, M., Hutley, L.B., Calders, K., Levick, S.R., 2023. Reduced model complexity for efficient characterisation of savanna woodland structure using terrestrial laser scanning. Int. J. Appl. Earth Obs. Geoinf. 118, 103255. https://doi.org/10.1016/j.jag.2023.103255.
Lumley, T., 2020. Leaps: Regression Subset Selection. https://CRAN.R-project.org/package=leaps.
Massey, A., Mandallaz, D., Lanz, A., 2014. Integrating remote sensing and past inventory data under the new annual design of the Swiss National Forest Inventory using three-phase design-based regression estimation. Can. J. For. Res. 44 (10), 1177–1186. https://doi.org/10.1139/cjfr-2014-0152.
Matérn, B., 1960. Spatial variation: Stochastic models and their application to some problems in forest surveys and other sampling investigations. Skoksforskninstitut, Band 49. Nr 5, 144–p.
McGaughey, R.J., 2019. FUSION/LDV: Software for LiDAR Data Analysis and Visualization (Version 3.80). Seattle, WA. Available online: http://forsys.cfr.washington.edu/fusion/fusionlatest.html.
McRoberts, R.E., 2006. A model-based approach to estimating forest area. Remote Sens. Environ. 103 (1), 56–66. https://doi.org/10.1016/J.RSE.2006.03.005.
McRoberts, R.E., 2010. Probability- and model-based approaches to inference for proportion forest using satellite imagery as ancillary data. Remote Sens. Environ. 114 (5), 1017–1025. https://doi.org/10.1016/J.RSE.2009.12.013.
McRoberts, R.E., Næsset, E., Gobakken, T., 2013. Inference for lidar-assisted estimation of forest growing stock volume. Remote Sens. Environ. 128, 268–275. https://doi.org/10.1016/J.RSE.2012.10.007.
McRoberts, R.E., Andersen, H.-E., Næsset, E., 2014. Using airborne laser scanning data to support forest sample surveys. In: Forestry Applications of Airborne Laser Scanning: Concepts and Case Studies, pp. 269–292. https://doi.org/10.1007/978-94-017-8663-8_14.
McRoberts, R.E., Næsset, E., Heikkinen, J., Chen, Q., Strimbu, V., Esteban, J., Chirici, G., 2022. On the model-assisted regression estimators using remotely sensed auxiliary data. Remote Sens. Environ. 281, 113168. https://doi.org/10.1016/j.rse.2022.113168.
McRoberts, R.E., Næsset, E., Heikkinen, J., Strimbu, V., 2024. Two-stage, model-assisted estimation using remotely sensed auxiliary data. Remote Sens. Environ. 307, 114125. https://doi.org/10.1016/j.rse.2024.114125.
Molina-Valero, J.A., Martínez-Calvo, A., Ginzo Villamayor, M.J., Novo Pérez, M.A., Álvarez-González, J.G., Montes, F., Pérez-Cruzado, C., 2022. Operationalizing the use of TLS in forest inventories: the R package FORTLS. Environ. Model Softw. 150, 105337. https://doi.org/10.1016/J.ENVSOFT.2022.105337.
Næsset, E., Gobakken, T., Bollandsås, O.M., Gregoire, T.G., Nelson, R., Ståhl, G., 2013. Comparison of precision of biomass estimates in regional field sample surveys and airborne LiDAR-assisted surveys in Hedmark County, Norway. Remote Sens. Environ. 130, 108–120. https://doi.org/10.1016/J.RSE.2012.11.010.
Newnham, G.J., Armston, J.D., Calders, K., Disney, M.I., Lovell, J.L., Schaaf, C.B., Strahler, A.H., Mark Danson, F., 2015. Terrestrial laser scanning for plot-scale forest measurement. Curr. For. Rep. 1 (4), 239–251. https://doi.org/10.1007/s40725-015-0025-5.
Persson, H.J., Olofsson, K., Holmgren, J., 2022. Two-phase forest inventory using very-high-resolution laser scanning. Remote Sens. Environ. 271, 112909. https://doi.org/10.1016/J.RSE.2022.112909.
Puliti, S., Ørka, H.O., Gobakken, T., Næsset, E., 2015. Inventory of small forest areas using an unmanned aerial system. Remote Sens 7 (8), 9632–9654. https://doi.org/10.3390/rs70809632.
Puliti, S., Ene, L.T., Gobakken, T., Næsset, E., 2017. Use of partial-coverage UAV data in sampling for large scale forest inventories. Remote Sens. Environ. 194, 115–126. https://doi.org/10.1016/J.RSE.2017.03.019.
Puliti, S., Saarela, S., Gobakken, T., Ståhl, G., Næsset, E., 2018. Combining UAV and Sentinel-2 auxiliary data for forest growing stock volume estimation through hierarchical model-based inference. Remote Sens. Environ. 204, 485–497. https://doi.org/10.1016/J.RSE.2017.10.007.
Puliti, S., Dash, J.P., Watt, M.S., Breidenbach, J., Pearse, G.D., 2020. A comparison of UAV laser scanning, photogrammetry and airborne laser scanning for precision

inventory of small-forest properties. Forestr.: Int. J. Forest Res. 93 (1), 150–162. https://doi.org/10.1093/forestry/cpz057.
R Core Team, 2023. R: A Language and Environment for Statistical Computing. R Foundation for Statistical Computing, Vienna, Austria. https://www.R-project.org/.
Roussel, J., Auty, D., 2023. Airborne LiDAR Data Manipulation and Visualization for Forestry Applications (R Package Version 4.0.4). https://cran.r-project.org/package=lidR.
Roussel, J.R., Auty, D., Coops, N.C., Tompalski, P., Goodbody, T.R.H., Meador, A.S., Bourdon, J.F., de Boissieu, F., Achim, A., 2020. lidR: an R package for analysis of airborne laser scanning (ALS) data. Remote Sens. Environ. 251, 112061. https://doi.org/10.1016/J.RSE.2020.112061.
Saarela, S., Grafström, A., Ståhl, G., Kangas, A., Holopainen, M., Tuominen, S., Nordkvist, K., Hyyppä, J., 2015a. Model-assisted estimation of growing stock volume using different combinations of LiDAR and Landsat data as auxiliary information. Remote Sens. Environ. 158, 431–440. https://doi.org/10.1016/J.RSE.2014.11.020.
Saarela, S., Schnell, S., Grafström, A., Tuominen, S., Nordkvist, K., Hyyppä, J., Kangas, A., Ståhl, G., 2015b. Effects of sample size and model form on the accuracy of model-based estimators of growing stock volume. Can. J. For. Res. 45 (11), 1524–1534. https://doi.org/10.1139/cjfr-2015-0077.
Saarela, S., Holm, S., Grafström, A., Schnell, S., Næsset, E., Gregoire, T.G., Nelson, R.F., Ståhl, G., 2016. Hierarchical model-based inference for forest inventory utilizing three sources of information. Ann. For. Sci. 73 (4), 895–910. https://doi.org/10.1007/S13595-016-0590-1.
Saarela, S., Breidenbach, J., Raumonen, P., Grafström, A., Ståhl, G., Ducey, M.J., Astrup, R., 2017. Kriging prediction of stand-level forest information using mobile laser scanning data adjusted for nondetection. Can. J. For. Res. 47 (9), 1257–1265. https://doi.org/10.1139/cjfr-2017-0019.
Saarela, S., Holm, S., Healey, S.P., Andersen, H.E., Petersson, H., Prentius, W., Ståhl, G., 2018. Generalized hierarchical model-based estimation for aboveground biomass assessment using GEDI and Landsat data. Remote Sens. 10 (11), 1832. https://doi.org/10.3390/rs10111832.
Saarela, S., Varvia, P., Korhonen, L., Yang, Z., Patterson, P.L., Gobakken, T., Ståhl, G., 2023. Three-phase hierarchical model-based and hybrid inference. MethodsX 11, 102321. https://doi.org/10.1016/j.mex.2023.102321.
Särndal, C.E., Swensson, B., Wretman, J., 1992. Model Assisted Survey Sampling. Springer-Verlag.
Seidel, D., Ammer, C., 2014. Efficient measurements of basal area in short rotation forests based on terrestrial laser scanning under special consideration of shadowing. iForest-Biogeosci. Forestr. 7 (4), 227. https://doi.org/10.3832/ifor1084-007.
Srinivasan, S., Popescu, S.C., Eriksson, M., Sheridan, R.D., Ku, N.W., 2015. Terrestrial laser scanning as an effective tool to retrieve tree level height, crown width, and stem diameter. Remote Sensing 7 (2), 1877–1896. https://doi.org/10.3390/RS70201877.
Stovall, A.E.L., Vorster, A., Anderson, R., Evangelista, P., 2023. Developing nondestructive species-specific tree allometry with terrestrial laser scanning. Methods Ecol. Evol. 14 (1), 280–290. https://doi.org/10.1111/2041-210X.14027.
Strunk, J.L., Reutebuch, S.E., Andersen, H.E., Gould, P.J., McGaughey, R.J., 2012. Model-assisted forest yield estimation with light detection and ranging. West. J. Appl. For. 27 (2), 53–59. https://doi.org/10.5849/WJAF.10-043.
Tillé, Y., Wilhelm, M., 2017. Probability sampling designs: principles for choice of design and balancing. Stat. Sci. 32 (2), 176–189. https://doi.org/10.1214/16-STS606.
Tompalski, P., Goodbody, T., 2021. Additional point cloud metrics to use with *_metric functions in lidR. https://github.com/ptompalski/lidRmetrics.
Trochta, J., Kruček, M., Vrška, T., Kraâl, K., 2017. 3D Forest: an application for descriptions of three-dimensional forest structures using terrestrial LiDAR. PLoS One 12 (5), e0176871. https://doi.org/10.1371/JOURNAL.PONE.0176871.
van Ewijk, K.Y., Treitz, P.M., Scott, N.A., 2011. Characterizing forest succession in Central Ontario using LiDAR-derived indices. Photogrammetric Engineering & Remote Sens. 77 (3), 261–269. https://doi.org/10.14358/PERS.77.3.261.
Vatandaşlar, C., Seki, M., Zeybek, M., 2023. Assessing the potential of mobile laser scanning for stand-level forest inventories in near-natural forests. Forestr.: Int. J. Forest Res. 96 (4), 448–464. https://doi.org/10.1093/forestry/cpad016.
White, J.C., Coops, N.C., Wulder, M.A., Vastaranta, M., Hilker, T., Tompalski, P., 2016. Remote sensing technologies for enhancing forest inventories: a review. Can. J. Remote. Sens. 42 (5), 619–641. https://doi.org/10.1080/07038992.2016.1207484.
Wulder, M.A., White, J.C., Nelson, R.F., Næsset, E., Ørka, H.O., Coops, N.C., Hilker, T., Bater, C.W., Gobakken, T., 2012. Lidar sampling for large-area forest characterization: a review. Remote Sens. Environ. 121, 196–209. https://doi.org/10.1016/J.RSE.2012.02.001.
Zhang, K., Chen, S.C., Whitman, D., Shyu, M.L., Yan, J., Zhang, C., 2003. A progressive morphological filter for removing nonground measurements from airborne LIDAR data. IEEE Trans. Geosci. Remote Sens. 41 (4), 872–882. https://doi.org/10.1109/TGRS.2003.810682.
Zhang, W., Qi, J., Wan, P., Wang, H., Xie, D., Wang, X., Yan, G., 2016. An easy-to-use airborne LiDAR data filtering method based on cloth simulation. Remote Sens. 8 (6), 501. https://doi.org/10.3390/rs8060501.